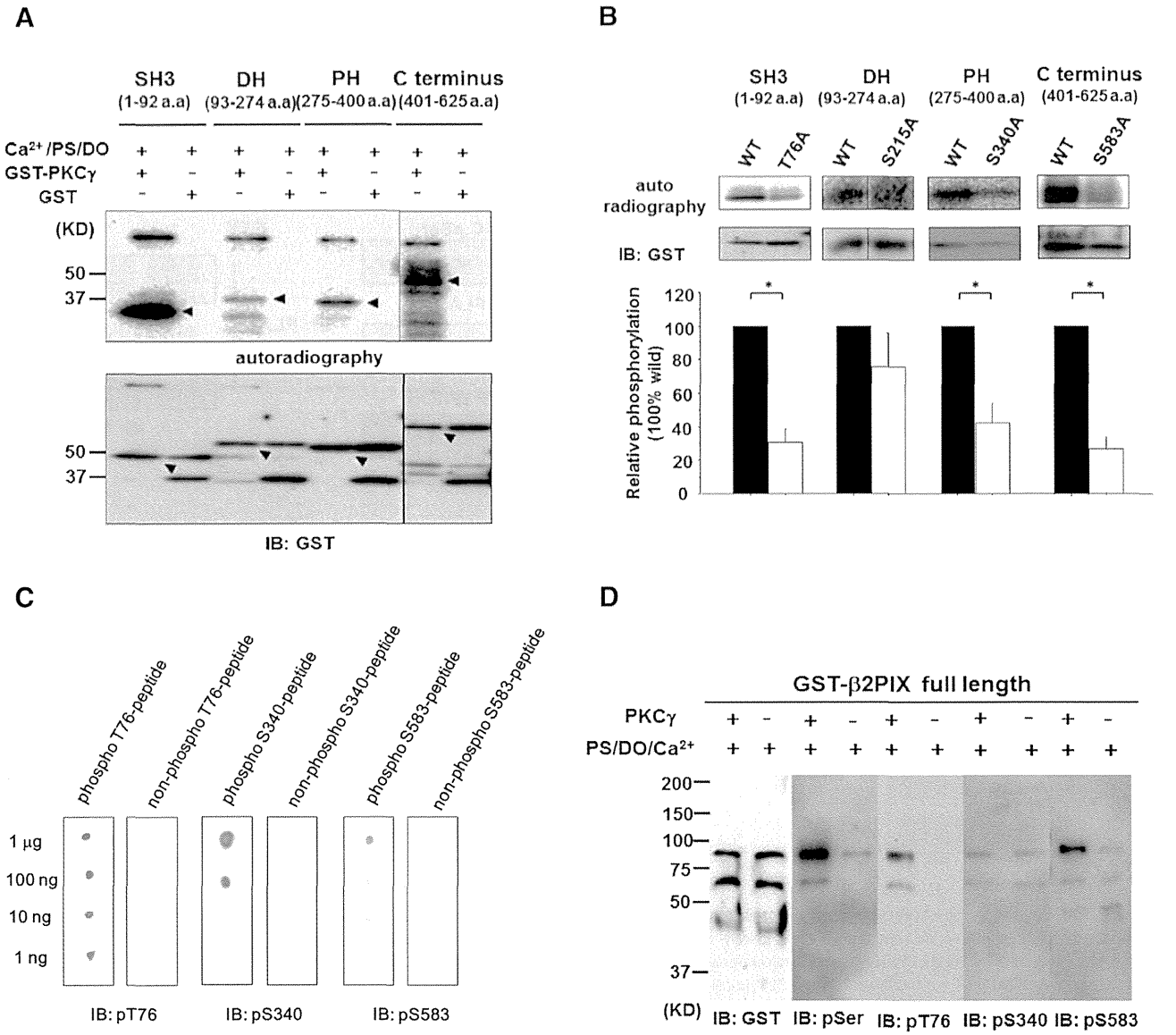

Figure 4. Analysis of the *in vitro* PKCγ phosphorylation sites in β2PIX. ***A***, *In vitro* phosphorylation of the GST-tagged β2PIX SH3, DH, PH, and C terminus regions. Each protein region was expressed in *E. coli*, purified, and incubated with [γ^{32}P] ATP and recombinant PKCγ in the presence of Ca^{2+}, PS, and DO. The phosphorylated proteins were separated by SDS-PAGE and detected by autoradiography (top). The protein levels of the recombinant β2PIX protein regions were detected by Western blotting (bottom). The arrowheads on the top indicate the autoradiography and those on the bottom indicate the total protein for each domain. ***B***, *In vitro* phosphorylation of the β2PIX SH3, DH, PH, and β2 C terminus regions containing the indicated mutations determined by an *in vitro* phosphorylation assay that was followed by mass spectrometry and phosphoproteome analysis. Phosphorylation levels were normalized to the WT phosphorylation signal for each domain, which were set to 100%: SH3 ($n = 5$), DH ($n = 4$), PH ($n = 5$), β2 C terminus ($n = 3$); The results are expressed as mean ± SEM ($^*p < 0.05$, unpaired *t* test). ***C***, Specificity of anti-phospho-Thr76, Ser340, and Ser583 antibodies. The indicated amount of the phospho-peptide (pT76 [VSPKSG(pT)LKSPP], pS340 [SASPRM-(pS)GFIYQ], and pS583 [SLGRRS(pS)LSRLE]) or non-phosphopeptide was dotted on the PVDF membrane. Immunostaining was performed using purified anti-pT76, pS340, and pS583 antibodies. ***D***, *In vitro* phosphorylation assay of full-length β2PIX. GST-tagged full-length β2PIX was expressed in *E. coli*, purified, and incubated with ATP and recombinant PKCγ in the presence of Ca^{2+}, PS, and DO. Phosphorylated proteins were separated by SDS-PAGE and detected by an anti-pSer PKC motif antibody, an anti-pT76 antibody, an anti-pS340 antibody, or an anti-pS583 antibody, respectively.

pairment. To identify the substrates for PKCγ, we performed a phosphoproteome analysis using HAMMOC methods (Kyono et al., 2008; Fig. 2*A*). Among the phosphopeptides in the WT group, we chose the proteins that may have a relationship to exocytosis and then calculated the WT/KO ratio of the average ion intensity. The average ion intensity ratio of the phosphopeptides that included the PKC phosphorylation motif are shown in Table 2. Among these 10 candidates, we focused on βPIX (Fig. 2*B*), even when the degree of the phosphorylation decrease was small, because it is expressed in DAergic neurons in the SNpc (http://www.informatics.jax.org/assay/MGI:4944920) and has been reported to play important roles in the machinery of exocytosis (Audebert et al., 2004; Momboisse et al., 2009). In the present phosphoproteome analysis, phosphorylation of Ser340 in β2PIX was detected. The βPIX family consists of two splicing forms, β1 and β2; the difference between β1 and β2 PIX exists in the C terminus (Fig. 2*C*). Although both β1 and β2 contain Ser340, β2PIX is the predominant form in the CNS (Koh et al., 2001). Therefore, β2PIX was used in the present study.

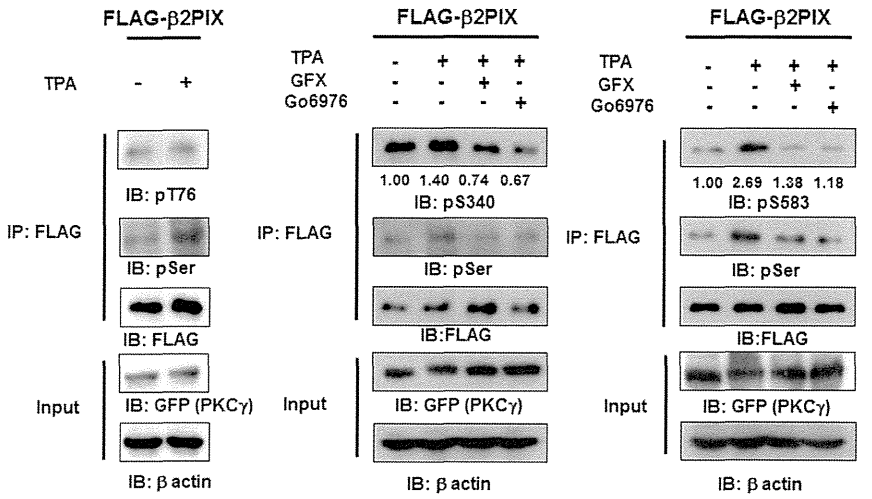

Figure 5. PKC mediates the phosphorylation of full-length β2PIX at Ser340 and Ser583 in cells. HEK293 cells transfected with FLAG-tagged WT β2PIX and GFP-tagged PKCγ were stimulated with 1 μM TPA in the presence or absence of 1 μM GFX, which is a pan-PKC inhibitor, or Gö6976, which is a cPKC inhibitor. FLAG-tagged β2PIX was precipitated and separated by SDS-PAGE. The total amounts of protein were determined by immunoblot analyses with an anti-FLAG antibody. GFP-tagged PKCγ or β actin was detected by anti-GFP or anti-β-actin antibodies. The phosphorylation levels of the FLAG-tagged β2PIX proteins that were determined with an anti-pT76 antibody (***A***; $n = 2$), an anti-pS340 (***B***; $n = 4$), or an anti-pS583 (***C***; $n = 4$) antibody were normalized to the phosphorylation levels of the WT. The numbers show the average relative phosphorylation levels that were normalized to prestimulation levels set as 1.00.

βPIX is phosphorylated by PKCγ *in vitro*, in cells, and *in vivo*

To determine whether β2PIX was phosphorylated by PKCγ, we performed *in vitro*, in cells, and *in vivo* phosphorylation experiments. β2PIX was phosphorylated by PKCγ *in vitro*, whereas the inhibition of PKC activity with GFX abolished the phosphorylation (Fig. 3*A*). Next, we investigated whether β2PIX was phosphorylated by PKC in cells. Enhanced phosphorylation of FLAG-tagged β2PIX extracted from HEK293 cells transfected with FLAG-tagged β2PIX and GFP-tagged PKCγ after treatment with 1 μM TPA was observed with an anti-Ser PKC motif Ab (Fig. 3*B*). Furthermore, the TPA-induced phosphorylation of β2PIX in cells was reduced by the PKC inhibitors Gö6976 and GFX (Fig. 3*B*). These results were further confirmed in PC12 cells (Fig. 3*C*) and in the P2 synaptosomal fraction of the mouse brain (Fig. 3*D*). Collectively, these results showed that β2PIX was phosphorylated by Ca^{2+}-dependent PKC *in vitro*, in cells, and *in vivo*.

PKCγ phosphorylates Thr76 in SH3, Ser340 in PH, and Ser583 in the C terminus of β2PIX *in vitro*

β2PIX consists of the following four regions: SH3 (1–92 aa), DH (93–274 aa), PH (275–400 aa), and the C terminus (401–625 aa). Because each region of β2PIX contains one or more predicted PKC phosphorylation sites, we performed an MS analysis combined with an in vitro phosphorylation assay using full-length GST-tagged β2PIX for screening the phosphorylation sites by PKCγ. The *in vitro* PKC assay, followed by the MS analysis, revealed the phosphorylation of Thr76, Ser215, and Ser583 in addition to that of Ser340, which was revealed by the phosphoproteome analysis of PKCγ KO mice (Fig. 2*C*). Thr76, Ser215, and Ser340 are common sites in both β1 and β2PIX. However, Ser583 is found only in β2PIX. To examine the PKCγ-mediated phosphorylation of these sites, recombinant proteins were used in *in vitro* phosphorylation assays. Importantly, all domains of β2PIX were phosphorylated by PKCγ *in vitro*, but the SH3 and C-terminal domains were phosphorylated much more strongly than the DH and PH domains (Fig. 4*A*). For the next step, we generated recombinant mutant proteins in which each Ser or Thr residue was replaced with Ala (Thr76Ala in SH3, Ser215Ala in DH, Ser340Ala in PH, and Ser583Ala in the C terminus) and examined which Ser/Thr residues of Thr76, Ser215, Ser340, or Ser583 could be phosphorylated by PKCγ *in vitro*. We observed that the Thr76Ala and Ser583Ala mutant proteins exhibited impaired phosphorylation of the SH3 and C-terminal domains (Fig. 4*B*). The Ser340Ala in the PH domain showed a moderately reduced phosphorylation. The Ser215Ala showed no significant reduction of phosphorylation in the DH domain. These findings suggested that Thr76, Ser340, and Ser583, but not Ser215, are PKCγ phosphorylation sites *in vitro*.

cPKC phosphorylates β2PIX Ser340 and Ser583 in cells

To further confirm that β2PIX is phosphorylated by cPKC in cells, we produced Abs that specifically recognized phosphorylated Thr76, Ser340, and Ser583 (Fig. 4*C*). The purified full-length β2PIX was phosphorylated by recombinant PKCγ *in vitro* and then applied to SDS-PAGE, which was followed by Western blotting with the anti-pT76, anti-pS340, and anti-pS583 Abs. The β2PIX that was phosphorylated by PKCγ was detected by anti-pT76 and anti-pS583, but not the anti-pS340 Ab (Fig. 4*D*), suggesting that Ser340 was not a direct PKC phosphorylation site. Next, we investigated whether β2PIX was phosphorylated at Thr76, Ser340, and Ser583 in cells. Figure 5 shows that Ser340 and Ser583, but not Thr76, were phosphorylated in TPA-treated HEK293 cells. Moreover, the PKC-dependent phosphorylation of Ser340 and Ser583 was confirmed with the PKC inhibitors Gö6976 and GFX (Fig. 5). These findings suggested that Ser340 and Ser583 were phosphorylated by cPKC in cells. It is noteworthy that Ser583 was phosphorylated directly, whereas Ser340 was phosphorylated indirectly by PKCγ.

Involvement of cPKC in the regulation of DA release

A ^{3}H-DA release assay in PC12 cells, a cell line in a DAergic neuronal model, was used to study the functional role of PKC and βPIX in the regulation of DA release. PC12 cells expressed endogenous βPIXs and cPKCs, including PKCγ (Fig. 6*A*). To determine the degree of DA release stimulated by K^+, PC12 cells were stimulated with various K^+ concentrations and the DA release was increased in a K^+ concentration-dependent manner (Fig. 6*B*). The functional role of cPKC in the regulation of K^+-induced DA release was monitored with Gö6976 and GFX. These PKC inhibitors significantly decreased the high K^+-stimulated DA release (Fig. 6*C*). It is noted that there were no differences of ^{3}H-DA uptake into the PC12 cells between the control and PKC inhibitor groups (Fig. 6*D*,*E*). Gö6976 and GFX also significantly suppressed the TPA-stimulated DA release (Fig. 6*F*). The activation of PKCγ after K^+-induced depolarization was confirmed by monitoring the translocation of GFP-tagged PKCγ from the cytosol to the plasma membrane in PC12 cells (Fig. 7*A*). These

results suggested that cPKC plays a crucial role in K^+-induced DA release machinery in PC12 cells.

βPIX KD suppressed DA release

Because βPIX is able to stimulate growth hormone secretion from PC12 cells (Momboisse et al., 2009; Momboisse et al., 2010), we investigated the possible relationship between βPIX and DA release. KD of βPIX in PC12 cells by shRNA (sh369) resulted in a significant inhibition of K^+-evoked DA secretion from PC12 cells (Fig. 7*B*). A similar significant reduction in DA release was reproduced with synthetic βPIX siRNA (Fig. 7*C*). These results were consistent with the idea that βPIX is an important element of the DA exocytotic machinery.

PKC-mediated phosphorylation of β2PIX at Ser340 and Ser583 promoted DA release

To determine the role of the PKC-mediated phosphorylation of βPIX in DA release, we exogenously and simultaneously introduced the shRNA-resistant forms of β2PIX mutant, including β2PIX Thr76Ala, Ser340Ala, or Ser583Ala mutants and βPIX sh369, into PC12 cells. DA release from PC12 cells transfected with sh369 was completely rescued by the reintroduction of WT FLAG-tagged β2PIX (Fig. 8*A*). These results suggested that β2PIX, which is a dominant isoform in the CNS, has important roles in DA release. Moreover, we examined the effects of the β2PIX phosphorylation on DA release. β2PIX Ser340Ala and Ser583Ala mutants failed to rescue the reduced DA release by βPIX sh369, whereas the β2PIX Thr76Ala mutant acted similarly to WT β2PIX (Fig. 8*A*). Together, our results suggested that the PKC-mediated phosphorylation of Ser340 and Ser583 on β2PIX positively regulates DA release. Finally, we examined the effects of Cdc42 and Rac1 KD on DA release. When Cdc42 was knocked down, Rac1 was upregulated and vice versa. Therefore, we knocked down both Cdc42 and Rac1. The KD of both Cdc42 and Rac1 in PC12 cells by shRNAs resulted in a significant inhibition of K^+-evoked DA release from PC12 cells (Fig. 8*B*).

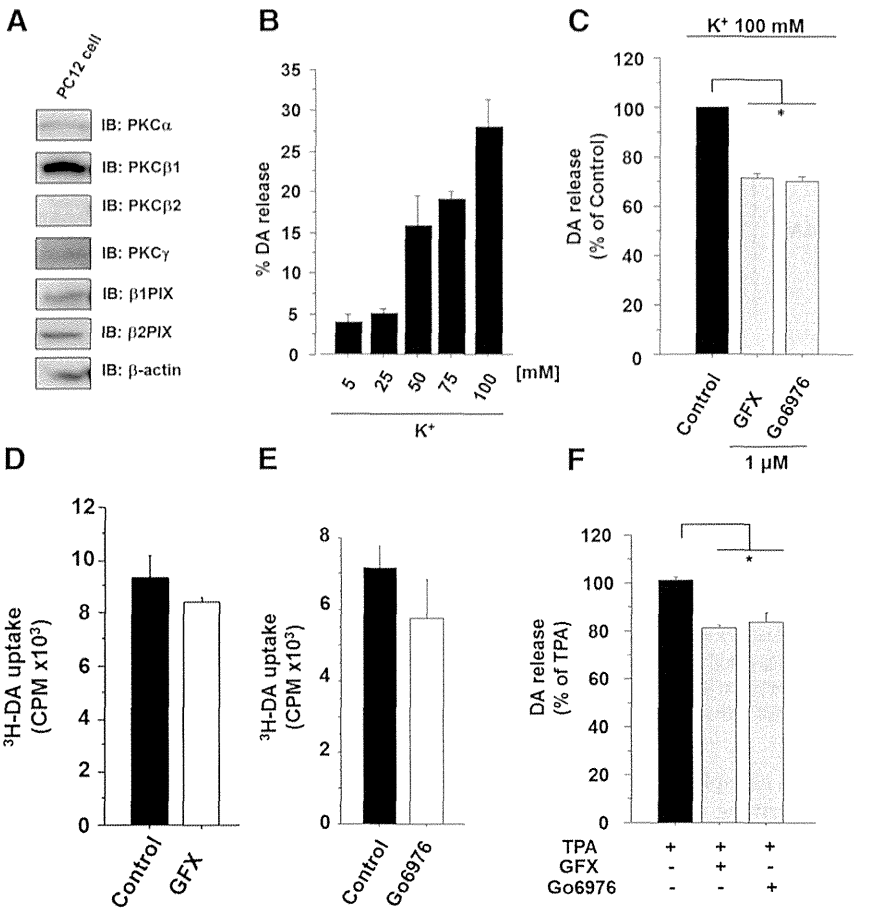

Figure 6. cPKC positively regulates K^+-stimulated DA release. ***A***, cPKCs and βPIX are expressed in PC12 cells. PC12 cell lysates were analyzed with immunoblotting with anti-PKCα, β1, β2, γ, and βPIX antibodies. ***B***, DA release in PC12 cells was measured with various K^+ concentrations. The results are expressed as mean ± SEM ($n = 3$). ***C***, Amounts of DA release that were stimulated in response to 100 mM K^+ with 1 μM GFX or 1 μM Gö6976 were measured in PC12 cells ($n = 3$; $^*p < 0.05$, unpaired *t* test). DA release levels were normalized to the levels released in response to 100 mM K^+, which were set to 100%. The results are expressed as mean ± SEM ($n = 3$–5). ***D***, ***E***, Uptake of ^{3}H-DA into PC12 cells with or without GFX and Gö6976 were measured. The results are expressed as mean ± SEM ($n = 3$). ***F***, TPA stimulated DA release in PC12 cells. DA release in PC12 cells was measured with 1 μM TPA in the absence or presence of 1 μM GFX. DA release levels were normalized to that of 1 μM TPA stimulation, which was set to 100%. The results are expressed as mean ± SEM ($n = 3$, $^*p < 0.01$, unpaired *t* test).

Discussion

In this study, we revealed that AS/AGU rats did not express full-length PKCγ or the truncated form of PKCγ, indicating that a loss, and not a gain, of function is the cause of the parkinsonian symptoms exhibited by AS/AGU rats. In agreement with these findings, we demonstrated decreased DA release stimulated by high levels of K^+ and METH in the striatum. It is noteworthy that altered DA release is the predominant characteristic of parkinsonian symptoms in PKCγ KO mice rather than loss of DAergic neurons in the SNpc. We propose that PKCγ KO animals are useful models for the study of parkinsonian syndrome because PKCγ KO mice and AS/AGU rats have damage not only in the DAergic system, but also in the serotonergic system (Al-Fayez et al., 2005), as has been observed in patients with sporadic Parkinson's disease. Furthermore, the use of the PKCγ KO mouse model has an advantage because it is possible to perform gene manipulations in them, such as PKCγ rescue, compared with the AS/AGU rats.

Although it is generally accepted that DA release in the striatum induced by high K^+ levels is mediated by exocytosis and not by DAT, PKC was reported to induce DAT endocytosis (Daniels and Amara, 1999), which, by altering DA reuptake, can change the amplitude of K^+-induced DA release as measured by microdialysis. We have ruled out this possibility because DAT activity was instead decreased in PKCγ KO mice (Fig. 1*F*). Moreover, ^{3}H-DA uptake does not differ between the control and PKC inhibitors in PC12 cells (Fig. 6*D*,*E*). These results suggested that the reduced K^+-induced DA release was not through the change of the DAT endocytosis by the PKCγ KO. There are also reports that activation of PKC induces DAT-mediated DA reverse transport (Kantor and Gnegy, 1998; Cowell et al., 2000). Although

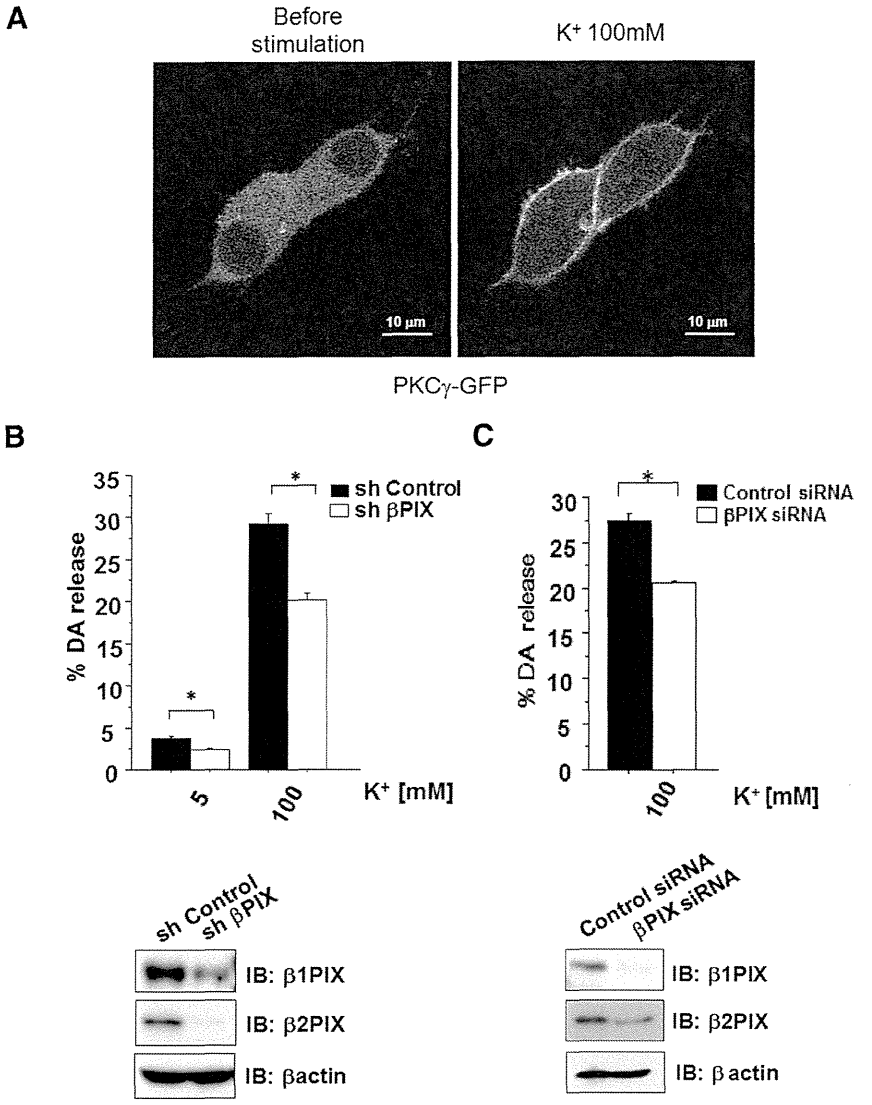

Figure 7. βPIX positively regulates K^+-stimulated DA release. ***A***, PKCγ was activated by high K^+ level stimulation in PC12 cells. Activation of PKCγ by K^+ stimulation was examined by monitoring the translocation of GFP-tagged PKCγ in PC12 cells. ***B***, DA release was measured in PC12 cells that were transfected with shRNA for βPIX and sh Control, which was used as a negative control. The results are expressed as mean ± SEM ($n = 6$, $^*p < 0.01$, *unpaired t* test). ***C***, DA release was measured in PC12 cells transfected with siRNA for βPIX. The expression of siRNAs for βPIX in PC12 cells and lysate was analyzed by immunoblot analyses with anti-βPIX antibodies. The results are expressed as mean ± SEM ($n = 5$, $^*p < 0.01$, unpaired *t* test).

these studies focused more on PKCβ than on PKCγ, our study showed that PKCγ also play important roles for DAT-mediated DA reverse transport (Fig. 1*F*), suggesting that PKCγ play roles for both K^+-mediated DA release and DAT-mediated DA reverse transport. Therefore, PKCγ KO resulted in decreased DAT activity, including uptaking DA and DA reverse transport through DAT. The decreased level of K^+-induced DA release in PKCγ KO mice is probably underestimated: DA release may be more significantly decreased when the disordered DAT activity is normalized.

We identified 10 phosphoproteins that were decreased in PKCγ KO mice under the hypothesis that decreased levels of phosphorylated substrates of PKCγ in the nigrostriatal system lead to impairments in DA release. Our results indicated that βPIX was one of the pivotal targets of PKCγ or cPKC in enhancing Ca^{2+}-evoked DA release based on the following several lines of evidence: (1) PKCγ phosphorylated βPIX *in vitro*, in cells, and *in vivo*; (2) Ser583 of βPIX was phosphorylated by PKCγ both *in vitro* and in cells, whereas Ser340 was phosphorylated by cPKC only in cells, suggesting that cPKC indirectly phosphorylated Ser340; (3) cPKC inhibitors and the KD of endogenous βPIX also suppressed the DA release from PC12 cells, suggesting that both PKCγ or cPKC and βPIX play pivotal roles in Ca^{2+}-evoked DA release from DAergic neurons; and (4) WT β2PIX, but not Ser340Ala or Ser583Ala, rescued the decreased DA release from PC12 cells by sh369 for βPIX, suggesting that both phosphorylation sites are necessary for regulating DA release. Why does PKCγ KO cause the parkinsonian syndrome phenotype, even when other cPKCs are expressed in PKCγ KO animals? Although the substrate specificity of each PKC subtype appears to be low *in vitro*, there have been several confirmatory reports of subtype-specific functions of cPKC under physiological conditions (Uchino et al., 2004; Ueyama et al., 2004; Al-Fayez et al., 2005; Kawasaki et al., 2010; Sakuma et al., 2012). Our data suggest that PKCγ has important roles in DA release in mice.

In neurons, Ca^{2+} entry triggers exocytosis, suggesting that certain Ca^{2+} sensors may be necessary for Ca^{2+}-dependent exocytosis. Candidates for Ca^{2+} sensors include molecules that possess EF hand motifs or C2 domains, which were first defined in cPKC, and annexin family proteins, as has been reported previously (Burgoyne and Morgan, 1998). PKC has been reported to modify exocytosis in the steps both before and after docking to the plasma membrane through the following mechanisms: (1) increased vesicle recruitment into the readily releasable pool (Gillis et al., 1996; Stevens and Sullivan, 1998), (2) acceleration of fusion pore expansion (Scepek et al., 1998), and (3) changes in the kinetics of exocytosis (Graham et al., 2002). However, βPIX is related to the exocytosis step after docking (Momboisse et al., 2009; Momboisse et al., 2010). The cPKC-βPIX-Cdc42/Rac1 axis possibly has important roles in DA release in the step after docking through the βPIX phosphorylation by cPKC.

How can βPIX regulate DA release through the phosphorylation at Ser340 or Ser583? Previous reports have revealed that βPIX phosphorylation results in βPIX translocation to the membrane and the subsequent activation of Rac1 and/or Cdc42. In PC12 cells, basic fibroblast growth factor induces the phosphorylation of βPIX at Ser525 and Thr526, resulting in neurite outgrowth by the activation of Rac1 through the translocation of the βPIX complex at neuronal growth cones (Shin et al., 2002; Shin et al., 2006). In human mesangial cells, endothelin-1 and cAMP inducers cause the PKA-dependent phosphorylation of βPIX at Ser516 and Thr526, resulting in cytoskeletal rearrangement by

the activation of Cdc42 through βPIX translocation (Chahdi et al., 2005). Therefore, βPIX may be differently phosphorylated in response to various stimuli and this may result in its stimulus-dependent specific targeting and Cdc42/Rac1 activation at the targeted sites. We have demonstrated for the first time that Ser583 is a PKCγ or cPKC phosphorylation site. Ser583 and the previously reported sites Ser516, Ser525, and Thr526 are all located in the C-terminal domain of βPIX and may have similar functions for the translocation and subsequent activation of Cdc42/Rac1. Phosphorylation at Ser340 is located in the PH domain, which interacts with phosphatidylinositol lipids within biological membranes (Wang and Shaw, 1995) and may also play important roles in the membrane targeting of βPIX. In fact, the PH domain has been reported to interact with PKC (Yao et al., 1994) and Cdc42 (Rossman et al., 2002) and it has been implicated in the regulation of the GEF activity of SOS (Ras-GEF; Karlovich et al., 1995) and p140Ras-GRF (Ras and Rac GEF; Buchsbaum et al., 1996). Therefore, through PH-domain-mediated membrane targeting and interaction, the cPKC-βPIX-Cdc42/Rac1 axis may act at specific membranes (Chen et al., 1997; Falasca et al., 1998; Maffucci and Falasca, 2001). Downstream of the βPIX phosphorylation, we speculate that Cdc42/Rac1 are the targets of phosphorylated βPIX, as suggested in previous studies (Shin et al., 2002; Shin et al., 2004; Chahdi et al., 2005; Shin et al., 2006). Although we have not proved a direct relationship between phosphorylated βPIX and Cdc42/Rac1, we speculate that βPIX phosphorylated by PKCγ regulates Cdc42/Rac1 functions based on our data that the double KD of Cdc42 and Rac1 resulted in decreased DA release (Fig. 8*B*).

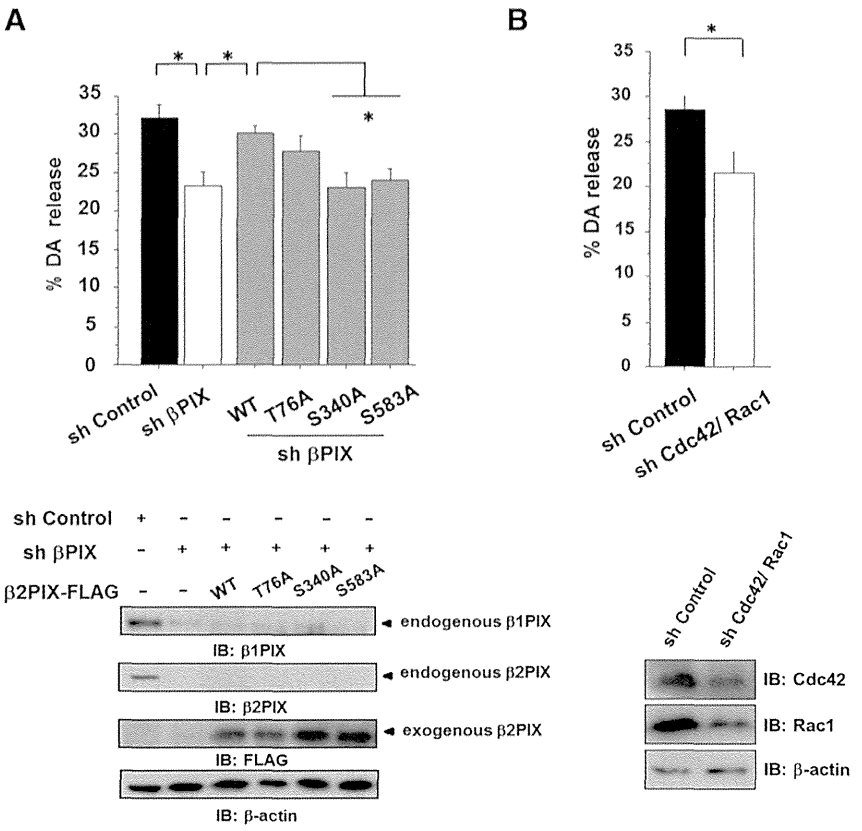

Figure 8. Phosphorylation of β2 PIX at Ser340 and Ser583 promotes DA release. ***A***, DA release was measured in PC12 cells that were transfected with shβPIX and β2PIX (WT and Ser-Ala mutants) with shRNA-resistant sequences. The levels of endogenous β1, β2PIX, and exogenous β2PIX were confirmed. Comparable levels of all ectopically expressed β2PIX proteins were confirmed by Western blot analyses. The results are expressed as mean ± SEM ($n = 3–6$, $^*p < 0.05$, one-way ANOVA with *post hoc* Dunnett's test). ***B***, DA release was measured in PC12 cells that were transfected with shRNA for both Cdc42 and Rac1 and sh Control, which was used as a negative control. The results are expressed as mean ± SEM ($n = 3$, $^*p < 0.01$, unpaired *t* test).

Although Ser340 is common to both β1PIX and β2PIX, Ser583 only exists in the unique C terminus of β2PIX, which is the neuron-dominant isoform (Koh et al., 2001) that emerged from and was conserved after *Xenopus laevis* (Fig. 9). Therefore, Ser583 phosphorylation by neuron-specific PKCγ may have important roles in the modulation of βPIX function in the highly developed CNS and highly elaborated function, including DA release. It is also of note that the reported phosphorylation sites at Ser340, Ser516, Ser525, and Thr526 are conserved through evolution. Although we detected the TPA-induced phosphorylation of β2PIX *in vivo* using the synaptosomal P2 fraction of PKCγ WT mice by pSer PKC motif Ab (Fig. 3*D*), we could not show clear TPA-induced phosphorylation at Ser340 and Ser583 in PKCγ WT using our site-specific phospho-Abs for pS340 and pS583, likely due to the sensitivity of anti-pS340 and pS583 Abs.

In the present study, we have demonstrated that PKCγ KO mice can be a useful model of parkinsonian syndrome. In addition, we found for the first time that DA release was positively regulated by the PKC-mediated direct phosphorylation of βPIX at Ser583 and indirect phosphorylation at Ser340. The phospho-

Figure 9. Schematic comparisons of Ser340 and Ser583 through evolution. Ser340 and Ser583 are evolutionally conserved in many species. It is noted that β2PIX emerged from *X. laevis*, although β1PIX is expressed in *Drosophila melanogaster*. Ser516, Ser525, and Thr526, as reported previously, are also conserved in many species.

rylational modulation of βPIX by PKCγ may be a potential therapeutic target for the treatment of parkinsonian syndrome.

References

Adachi N, Oyasu M, Taniguchi T, Yamaguchi Y, Takenaka R, Shirai Y, Saito N (2005) Immunocytochemical localization of a neuron-specific diacylglycerol kinase beta and gamma in the developing rat brain. Brain Res Mol Brain Res 139:288–299. CrossRef Medline

Ago Y, Araki R, Tanaka T, Sasaga A, Nishiyama S, Takuma K, Matsuda T (2013) Role of social encounter-induced activation of prefrontal serotonergic systems in the abnormal behaviors of isolation-reared mice. Neuropsychopharmacology 38:1535–1547. CrossRef Medline

Al-Fayez M, Russell D, Wayne Davies R, Shiels PG, Baker PJ, Payne AP (2005) Deficits in the mid-brain raphe nuclei and striatum of the AS/AGU rat, a protein kinase C-gamma mutant. Eur J Neurosci 22:2792–2798. CrossRef Medline

Audebert S, Navarro C, Nourry C, Chasserot-Golaz S, Lécine P, Bellaiche Y, Dupont JL, Premont RT, Sempéré C, Strub JM, Van Dorsselaer A, Vitale N, Borg JP (2004) Mammalian Scribble forms a tight complex with the betaPIX exchange factor. Curr Biol 14:987–995. CrossRef Medline

Barclay JW, Craig TJ, Fisher RJ, Ciufo LF, Evans GJ, Morgan A, Burgoyne RD (2003) Phosphorylation of Munc18 by protein kinase C regulates the kinetics of exocytosis. J Biol Chem 278:10538–10545. CrossRef Medline

Buchsbaum R, Telliez JB, Goonesekera S, Feig LA (1996) The N-terminal pleckstrin, coiled-coil, and IQ domains of the exchange factor Ras-GRF act cooperatively to facilitate activation by calcium. Mol Cell Biol 16:4888–4896. Medline

Burgoyne RD, Morgan A (1998) Calcium sensors in regulated exocytosis. Cell Calcium 24:367–376. CrossRef Medline

Campbell JM, Payne AP, Gilmore DP, Byrne JE, Russell D, McGadey J, Clarke DJ, Davies RW, Sutcliffe RG (1996) Neostriatal dopamine depletion and locomotor abnormalities due to the Albino Swiss rat agu mutation. Neurosci Lett 213:173–176. Medline

Chahdi A, Sorokin A (2008) Protein kinase A-dependent phosphorylation modulates beta1Pix guanine nucleotide exchange factor activity through 14–3-3beta binding. Mol Cell Biol 28:1679–1687. CrossRef Medline

Chahdi A, Miller B, Sorokin A (2005) Endothelin 1 induces beta 1Pix translocation and Cdc42 activation via protein kinase A-dependent pathway. J Biol Chem 280:578–584. CrossRef Medline

Chefer VI, Czyzyk T, Bolan EA, Moron J, Pintar JE, Shippenberg TS (2005) Endogenous kappa-opioid receptor systems regulate mesoaccumbal dopamine dynamics and vulnerability to cocaine. J Neurosci 25:5029–5037. CrossRef Medline

Chen RH, Corbalan-Garcia S, Bar-Sagi D (1997) The role of the PH domain in the signal-dependent membrane targeting of Sos. EMBO J 16:1351–1359. CrossRef Medline

Cowell RM, Kantor L, Hewlett GH, Frey KA, Gnegy ME (2000) Dopamine transporter antagonists block phorbol ester-induced dopamine release and dopamine transporter phosphorylation in striatal synaptosomes. Eur J Pharmacol 389:59–65. CrossRef Medline

Craig NJ, Durán Alonso MB, Hawker KL, Shiels P, Glencorse TA, Campbell JM, Bennett NK, Canham M, Donald D, Gardiner M, Gilmore DP, MacDonald RJ, Maitland K, McCallion AS, Russell D, Payne AP, Sutcliffe RG, Davies RW (2001) A candidate gene for human neurodegenerative disorders: a rat PKC gamma mutation causes a parkinsonian syndrome. Nat Neurosci 4:1061–1062. CrossRef Medline

Daniels GM, Amara SG (1999) Regulated trafficking of the human dopamine transporter: clathrin-mediated internalization and lysosomal degradation in response to phorbol esters. J Biol Chem 274:35794–35801. CrossRef Medline

Ding YQ, Xiang CX, Chen ZF (2005) Generation and characterization of the PKC gamma-Cre mouse line. Genesis 43:28–33. CrossRef Medline

Falasca M, Logan SK, Lehto VP, Baccante G, Lemmon MA, Schlessinger J (1998) Activation of phospholipase C gamma by PI 3-kinase-induced PH domain-mediated membrane targeting. EMBO J 17:414–422. CrossRef Medline

Feng Q, Baird D, Peng X, Wang J, Ly T, Guan JL, Cerione RA (2006) Cool-1 functions as an essential regulatory node for EGF receptor- and Src-mediated cell growth. Nat Cell Biol 8:945–956. CrossRef Medline

Franklin KBJ, Paxinos G (1997) The mouse brain in stereotaxic coordinates. San Diego: Academic.

Gillis KD, Mossner R, Neher E (1996) Protein kinase C enhances exocytosis from chromaffin cells by increasing the size of the readily releasable pool of secretory granules. Neuron 16:1209–1220. CrossRef Medline

Graham ME, O'Callaghan DW, McMahon HT, Burgoyne RD (2002) Dynamin-dependent and dynamin-independent processes contribute to the regulation of single vesicle release kinetics and quantal size. Proc Natl Acad Sci U S A 99:7124–7129. CrossRef Medline

Hewett J, Johanson P, Sharma N, Standaert D, Balcioglu A (2010) Function of dopamine transporter is compromised in DYT1 transgenic animal model in vivo. J Neurochem 113:228–235. CrossRef Medline

Hilfiker S, Pieribone VA, Nordstedt C, Greengard P, Czernik AJ (1999) Regulation of synaptotagmin I phosphorylation by multiple protein kinases. J Neurochem 73:921–932. CrossRef Medline

Iwasaki S, Kataoka M, Sekiguchi M, Shimazaki Y, Sato K, Takahashi M (2000) Two distinct mechanisms underlie the stimulation of neurotransmitter release by phorbol esters in clonal rat pheochromocytoma PC12 cells. J Biochem 128:407–414. CrossRef Medline

Justice JB Jr (1993) Quantitative microdialysis of neurotransmitters. J Neurosci Methods 48:263–276. CrossRef Medline

Kantor L, Gnegy ME (1998) Protein kinase C inhibitors block amphetamine-mediated dopamine release in rat striatal slices. J Pharmacol Exp Ther 284:592–598. Medline

Karlovich CA, Bonfini L, McCollam L, Rogge RD, Daga A, Czech MP, Banerjee U (1995) In vivo functional analysis of the Ras exchange factor son of sevenless. Science 268:576–579. CrossRef Medline

Kawasaki T, Ishihara K, Ago Y, Nakamura S, Itoh S, Baba A, Matsuda T (2006) Protective effect of the radical scavenger edaravone against methamphetamine-induced dopaminergic neurotoxicity in mouse striatum. Eur J Pharmacol 542:92–99. CrossRef Medline

Kawasaki T, Ishihara K, Ago Y, Baba A, Matsuda T (2007) Edaravone (3-methyl-1-phenyl-2-pyrazolin-5-one), a radical scavenger, prevents 1-methyl-4-phenyl-1,2,3,6-tetrahydropyridine-induced neurotoxicity in the substantia nigra but not the striatum. J Pharmacol Exp Ther 322:274–281. CrossRef Medline

Kawasaki T, Ueyama T, Lange I, Feske S, Saito N (2010) Protein kinase C-induced phosphorylation of Orai1 regulates the intracellular Ca^{2+} level via the store-operated Ca^{2+} channel. J Biol Chem 285:25720–25730. CrossRef Medline

Koda K, Ago Y, Cong Y, Kita Y, Takuma K, Matsuda T (2010) Effects of acute and chronic administration of atomoxetine and methylphenidate on extracellular levels of noradrenaline, dopamine and serotonin in the prefrontal cortex and striatum of mice. J Neurochem 114:259–270. CrossRef Medline

Koh CG, Manser E, Zhao ZS, Ng CP, Lim L (2001) Beta1PIX, the PAK-interacting exchange factor, requires localization via a coiled-coil region to promote microvillus-like structures and membrane ruffles. J Cell Sci 114:4239–4251. Medline

Kose A, Ito A, Saito N, Tanaka C (1990) Electron microscopic localization of gamma- and beta II-subspecies of protein kinase C in rat hippocampus. Brain Res 518:209–217. CrossRef Medline

Kyono Y, Sugiyama N, Imami K, Tomita M, Ishihama Y (2008) Successive and selective release of phosphorylated peptides captured by hydroxy acid-modified metal oxide chromatography. J Proteome Res 7:4585–4593. CrossRef Medline

Maffucci T, Falasca M (2001) Specificity in pleckstrin homology (PH) domain membrane targeting: a role for a phosphoinositide-protein cooperative mechanism. FEBS Lett 506:173–179. CrossRef Medline

Matsubara T, Ikeda M, Kiso Y, Sakuma M, Yoshino K, Sakane F, Merida I, Saito N, Shirai Y (2012) c-Abl tyrosine kinase regulates serum-induced nuclear export of diacylglycerol kinase α by phosphorylation at Tyr-218. J Biol Chem 287:5507–5517. CrossRef Medline

Mayhew MW, Jeffery ED, Sherman NE, Nelson K, Polefrone JM, Pratt SJ, Shabanowitz J, Parsons JT, Fox JW, Hunt DF, Horwitz AF (2007) Identification of phosphorylation sites in betaPIX and PAK1. J Cell Sci 120:3911–3918. CrossRef Medline

Momboisse F, Lonchamp E, Calco V, Ceridono M, Vitale N, Bader MF, Gasman S (2009) betaPIX-activated Rac1 stimulates the activation of phospholipase D, which is associated with exocytosis in neuroendocrine cells. J Cell Sci 122:798–806. CrossRef Medline

Momboisse F, Ory S, Ceridono M, Calco V, Vitale N, Bader MF, Gasman S (2010) The Rho guanine nucleotide exchange factors Intersectin 1L and β-Pix control calcium-regulated exocytosis in neuroendocrine PC12 cells. Cell Mol Neurobiol 30:1327–1333. CrossRef Medline

Murray D, Honig B (2002) Electrostatic control of the membrane targeting of C2 domains. Mol Cell 9:145–154. CrossRef Medline

Nishizuka Y (1988) The molecular heterogeneity of protein kinase C and its implications for cellular regulation. Nature 334:661–665. CrossRef Medline

Nishizuka Y (1992) Intracellular signaling by hydrolysis of phospholipids and activation of protein kinase C. Science 258:607–614. CrossRef Medline

Ota T, Suzuki Y, Nishikawa T, Otsuki T, Sugiyama T, Irie R, Wakamatsu A, Hayashi K, Sato H, Nagai K, Kimura K, Makita H, Sekine M, Obayashi M, Nishi T, Shibahara T, Tanaka T, Ishii S, Yamamoto J, Saito K, et al. (2004) Complete sequencing and characterization of 21,243 full-length human cDNAs. Nat Genet 36:40–45. CrossRef Medline

Payne AP, Campbell JM, Russell D, Favor G, Sutcliffe RG, Bennett NK, Davies RW, Stone TW (2000) The AS/AGU rat: a spontaneous model of disruption and degeneration in the nigrostriatal dopaminergic system. J Anat 196:629–633. CrossRef Medline

Rossman KL, Worthylake DK, Snyder JT, Siderovski DP, Campbell SL, Sondek J (2002) A crystallographic view of interactions between Dbs and Cdc42: PH domain-assisted guanine nucleotide exchange. EMBO J 21:1315–1326. CrossRef Medline

Saito H, Oda Y, Sato T, Kuromitsu J, Ishihama Y (2006) Multiplexed two-dimensional liquid chromatography for MALDI and nanoelectrospray ionization mass spectrometry in proteomics. J Proteome Res 5:1803–1807. CrossRef Medline

Saito N, Shirai Y (2002) Protein kinase C gamma (PKC gamma): function of neuron specific isotype. J Biochem 132:683–687. CrossRef Medline

Sakuma M, Shirai Y, Yoshino K, Kuramasu M, Nakamura T, Yanagita T, Mizuno K, Hide I, Nakata Y, Saito N (2012) Novel PKCα-mediated phosphorylation site(s) on cofilin and their potential role in terminating histamine release. Mol Biol Cell 23:3707–3721. CrossRef Medline

Scepek S, Coorssen JR, Lindau M (1998) Fusion pore expansion in horse eosinophils is modulated by Ca^{2+} and protein kinase C via distinct mechanisms. EMBO J 17:4340–4345. CrossRef Medline

Seki T, Adachi N, Ono Y, Mochizuki H, Hiramoto K, Amano T, Matsubayashi H, Matsumoto M, Kawakami H, Saito N, Sakai N (2005) Mutant protein kinase Cgamma found in spinocerebellar ataxia type 14 is susceptible to aggregation and causes cell death. J Biol Chem 280:29096–29106. CrossRef Medline

Shin EY, Shin KS, Lee CS, Woo KN, Quan SH, Soung NK, Kim YG, Cha CI, Kim SR, Park D, Bokoch GM, Kim EG (2002) Phosphorylation of p85 beta PIX, a Rac/Cdc42-specific guanine nucleotide exchange factor, via the Ras/ERK/PAK2 pathway is required for basic fibroblast growth factor-induced neurite outgrowth. J Biol Chem 277:44417–44430. CrossRef Medline

Shin EY, Woo KN, Lee CS, Koo SH, Kim YG, Kim WJ, Bae CD, Chang SI, Kim EG (2004) Basic fibroblast growth factor stimulates activation of Rac1 through a p85 betaPIX phosphorylation-dependent pathway. J Biol Chem 279:1994–2004. CrossRef Medline

Shin EY, Lee CS, Cho TG, Kim YG, Song S, Juhnn YS, Park SC, Manser E, Kim EG (2006) betaPak-interacting exchange factor-mediated Rac1 activation requires smgGDS guanine nucleotide exchange factor in basic fibroblast growth factor-induced neurite outgrowth. J Biol Chem 281:35954–35964. CrossRef Medline

Stevens CF, Sullivan JM (1998) Regulation of the readily releasable vesicle pool by protein kinase C. Neuron 21:885–893. CrossRef Medline

ten Klooster JP, Jaffer ZM, Chernoff J, Hordijk PL (2006) Targeting and activation of Rac1 are mediated by the exchange factor beta-Pix. J Cell Biol 172:759–769. CrossRef Medline

Uchino M, Sakai N, Kashiwagi K, Shirai Y, Shinohara Y, Hirose K, Iino M, Yamamura T, Saito N (2004) Isoform-specific phosphorylation of metabotropic glutamate receptor 5 by protein kinase C (PKC) blocks Ca^{2+} oscillation and oscillatory translocation of Ca^{2+}-dependent PKC. J Biol Chem 279:2254–2261. CrossRef Medline

Ueyama T, Lennartz MR, Noda Y, Kobayashi T, Shirai Y, Rikitake K, Yamasaki T, Hayashi S, Sakai N, Seguchi H, Sawada M, Sumimoto H, Saito N (2004) Superoxide production at phagosomal cup/phagosome through βI protein kinase C during FcγR-mediated phagocytosis in microglia. J Immunol 173:4582–4589. CrossRef Medline

Ueyama T, Geiszt M, Leto TL (2006) Involvement of Rac1 in activation of multicomponent Nox1- and Nox3-based NADPH oxidases. Mol Cell Biol 26:2160–2174. CrossRef Medline

Ueyama T, Sakaguchi H, Nakamura T, Goto A, Morioka S, Shimizu A, Nakao K, Hishikawa Y, Ninoyu Y, Kassai H, Suetsugu S, Koji T, Fritzsch B, Yonemura S, Hisa Y, Matsuda M, Aiba A, Saito N (2014) Maintenance of stereocilia and apical junctional complexes by Cdc42 in cochlear hair cells. J Cell Sci 127:2040–2052. CrossRef Medline

Wang DS, Shaw G (1995) The association of the C-terminal region of beta I sigma II spectrin to brain membranes is mediated by a PH domain, does not require membrane proteins, and coincides with a inositol-1,4,5 triphosphate binding site. Biochem Biophys Res Commun 217:608–615. CrossRef Medline

Wu WC, Walaas SI, Nairn AC, Greengard P (1982) Calcium/phospholipid regulates phosphorylation of a Mr "87k" substrate protein in brain synaptosomes. Proc Natl Acad Sci U S A 79:5249–5253. CrossRef Medline

Yao L, Kawakami Y, Kawakami T (1994) The pleckstrin homology domain of Bruton tyrosine kinase interacts with protein kinase C. Proc Natl Acad Sci U S A 91:9175–9179. CrossRef Medline

nature COMMUNICATIONS

ARTICLE

Received 9 Sep 2013 | Accepted 11 Apr 2014 | Published 29 May 2014

DOI: 10.1038/ncomms4932 OPEN

TRPV2 is critical for the maintenance of cardiac structure and function in mice

Yuki Katanosaka[1], Keiichiro Iwasaki[1], Yoshihiro Ujihara[1,2], Satomi Takatsu[1], Koki Nishitsuji[1], Motoi Kanagawa[3], Atsushi Sudo[3], Tatsushi Toda[3], Kimiaki Katanosaka[4,5], Satoshi Mohri[1,2] & Keiji Naruse[1,6]

The heart has a dynamic compensatory mechanism for haemodynamic stress. However, the molecular details of how mechanical forces are transduced in the heart are unclear. Here we show that the transient receptor potential, vanilloid family type 2 (TRPV2) cation channel is critical for the maintenance of cardiac structure and function. Within 4 days of eliminating TRPV2 from hearts of the adult mice, cardiac function declines severely, with disorganization of the intercalated discs that support mechanical coupling with neighbouring myocytes and myocardial conduction defects. After 9 days, cell shortening and Ca^{2+} handling by single myocytes are impaired in TRPV2-deficient hearts. TRPV2-deficient neonatal cardiomyocytes form no intercalated discs and show no extracellular Ca^{2+}-dependent intracellular Ca^{2+} increase and insulin-like growth factor (IGF-1) secretion in response to stretch stimulation. We further demonstrate that IGF-1 receptor/PI3K/Akt pathway signalling is significantly downregulated in TRPV2-deficient hearts, and that IGF-1 administration partially prevents chamber dilation and impairment in cardiac pump function in these hearts. Our results improve our understanding of the molecular processes underlying the maintenance of cardiac structure and function.

[1] Department of Cardiovascular Physiology, Graduate School of Medicine, Dentistry and Pharmaceutical Sciences, Okayama University, Shikata-cho 2-5-1, Okayama city, Okayama 700-8558, Japan. [2] Department of Physiology, Kawasaki Medical School, Matsushima 577, Kurashiki, Okayama 701-0192, Japan. [3] Division of Neurology/Molecular Brain Science, Kobe University Graduate School of Medicine, Kobe 650-0017, Japan. [4] Department of Neuroscience II, Research Institute of Environmental Medicine, Nagoya University, Furo-cho, Chikusa-ku, Nagoya, Aichi 464-8601, Japan. [5] College of Life and Health Sciences, Chubu University, Matsumoto-cho 1200, Kasugai, Aichi 487-8501, Japan. [6] ICORP-SORST-Cell Mechanosensing Project, Japan Science and Technology Agency, Nagoya, Aichi 466-8550, Japan. Correspondence and requests for materials should be addressed to Y.K. (email: ytanigu@md.okayama-u.ac.jp).

Mechanical forces provide essential physiological information for homeostatic regulation and functional adaptation at the levels of cells and organs[1]. In cardiovascular systems, cellular mechanical responses to haemodynamic stress are crucial for normal cardiac function, and affect both the physiological and the pathological growth of the heart[2,3]. More specifically, an increased cardiac workload resulting from exercise, pregnancy or postnatal growth promotes the physiological growth of the heart, whereas chronic hypertension can cause pathological hypertrophy[3]. Atrophy of the heart is a complication of protracted bed rest, prolonged weightlessness during space travel, and mechanical unloading with a ventricular assist device[3]. Despite the obvious influence of mechanical load on cardiac structure and function, the molecular details of the myocardial mechanotransduction required to maintain cardiac structure and function have remained unclear.

The heart is a functional syncytium composed of terminally differentiated myocytes specialized for excitation–contraction (E–C) coupling[3]. Individual cardiomyocytes are electrically and mechanically coupled at their termini, where highly organized cell–cell junctions known as intercalated discs are located[4–6]. The structure of intercalated discs is known to be remodelled in response to haemodynamic stress[7]. High wall stress increases the myocardial contractile force exerted as a result of cardiac hypertrophy, and the intercalated disc structure has to be optimized for physical robustness to adapt to this force[3]. By contrast, mechanical unloading causes cardiac atrophy, accompanied by disorder in the intercalated disc structure[7–10]. In addition, human cardiomyopathies have been associated with mutations in genes encoding components of intercalated discs, involved in mechanical coupling, and studies in mice and humans have suggested a connection between faulty myocardial mechanical coupling mechanisms and heart disease[11–15]. Flexibility in cardiac adaptation to haemodynamic stress probably requires the maintenance of intercalated disc structure and function by continuous monitoring of the mechanical stress at intercalated discs. Therefore, we hypothesized that cardiac mechanoreceptors at intercalated discs detect mechanical stress in the heart, maintaining myocardial structure and function in response to haemodynamic stress through the mechanical feedback system in cardiomyocytes.

Members of the transient receptor potential (TRP) cation channel family are potential candidates for the mechanoreceptors responding to tension, flow or changes in cell volume[16]. Previously, we reported that recombinant TRP, vanilloid family type 2 (TRPV2) can be activated by hypotonicity- and stretch-induced mechanical stimulation in ectopic expression systems[17,18]. Interestingly, TRPV2 is highly localized to mammalian cardiac intercalated discs, and its increased expression at the sarcolemma is observed in dystrophic human patients and animal models deficient in dystrophin or δ-sarcoglycan[17]. To elucidate the physiological role of cardiac TRPV2, we generated temporally controlled cardiac-specific TRPV2-deficient mice. Cardiac-specific TRPV2 elimination led to a severe decline in the heart's pump function with the disorganization of the intercalated disc structure, conduction defects and accelerated mortality. TRPV2-deficient neonatal cardiomyocytes formed no intercalated discs and showed no extracellular Ca^{2+}-dependent intracellular Ca^{2+} increase and IGF-1 secretion after stretch stimulation. TRPV2-deficient hearts showed downregulation of IGF-1 receptor/PI3K/Akt signalling. In addition, IGF-1 administration partially prevented chamber dilation and improved cardiac pump function in TRPV2-deficient hearts. These results suggest an indispensable role for TRPV2 in the maintenance of cardiac structure and function.

Results

Generation of cardiac-specific TRPV2-deficient mice. Initially, mice carrying a *TRPV2*$^{flox/flox}$ allele were generated by flanking exon 4 of the *TRPV2* gene with two *loxP* sequences (Supplementary Fig. 1). Excision of this segment resulted in a frameshift mutation downstream of the deletion sites. Translation from the first ATG gave rise to a short, 92 amino-acid (aa) product containing 62 aa of the original TRPV2 protein; however, most of the TRPV2 channel structure was lost after *Cre*-mediated recombination. We crossed mice bearing the *TRPV2*$^{flox/flox}$ allele with a transgenic line (*MerCreMer*) expressing *Cre* recombinase under the control of the α-myosin heavy chain promoter in a tamoxifen-inducible cardiomyocyte-specific manner[19] to produce *TRPV2*$^{flox/flox}$;*MerCreMer*$^{+/-}$ mice. To account for the deleterious effect of potential nonspecific *Cre* recombinase-mediated cardiotoxicity[20], we used *TRPV2*$^{flox/+}$; *MerCreMer*$^{+/-}$ and *TRPV2*$^{flox/flox}$;*MerCreMer*$^{-/-}$ littermates as age-matched controls, from which *TRPV2*$^{flox/flox}$; *MerCreMer*$^{+/-}$ mice were indistinguishable in appearance. The *TRPV2*$^{flox/flox}$;*MerCreMer*$^{+/-}$ mice were genotyped by PCR using primers for *Cre-loxP* sites and *Cre* recombinase (Fig. 1a and Supplementary Fig. 1). In adult *TRPV2*$^{flox/flox}$; *MerCreMer*$^{+/-}$ mice treated with tamoxifen for 3 days (daily dose of 8 mg kg^{-1}), we confirmed successful *Cre* recombination by PCR amplification of cardiac genomic DNA, to detect the deleted allele (Fig. 1b). Consistently, the expression of TRPV2 messenger RNA was dramatically suppressed in the hearts of TRPV2-deficient mice on day 3 (Fig. 1c). There was an ~95% reduction in TRPV2 protein in membrane extracts of cardiac muscle from these mice after 4 days of tamoxifen treatment (Fig. 1d). Consistently, the TRPV2 protein was also not detectable by immunofluorescent staining at intercalated discs in the hearts of these mice, although TRPV2 was highly localized to intercalated discs in control mice (Fig. 1e). Hereafter, in this study, we treated *TRPV2*$^{flox/flox}$;*MerCreMer*$^{+/-}$, *TRPV2*$^{flox/+}$; *MerCreMer*$^{+/-}$ and *TRPV2*$^{flox/flox}$;*MerCreMer*$^{-/-}$ mice with 8 mg kg^{-1} per day tamoxifen or vehicle for 4 consecutive days, then carried out analyses at different time points.

The chamber dilation in TRPV2-deficient hearts. Paraffin sections from TRPV2-deficient hearts were treated with Masson's trichrome stain and analysed histologically. After 4 days of tamoxifen treatment, hearts from *TRPV2*$^{flox/flox}$;*MerCreMer*$^{+/-}$ mice were morphologically normal with no incremental changes in the heart weight/body weight ratio or the cross-sectional area of the cardiomyocytes (Fig. 2a–d). However, 9 days after the onset of tamoxifen treatment, the chambers of the hearts from these mice were enlarged, as seen in the final phase of dilated cardiomyopathy (Fig. 2a). This dilation differed from ventricular hypertrophy as the ventricle wall was not thickened. As evidence of this, within 10 days of the onset of tamoxifen administration, the heart weight/body weight ratio and cardiomyocyte cross-sectional area in TRPV2-deficient hearts were comparable with those of control mice (Fig. 2b,c). In addition, the cardiomyocytes of TRPV2-deficient mice showed no cellular degeneration or intermuscular fibrosis (Fig. 2d). Whereas the cell–cell interfaces forming intercalated discs ran perpendicular to the muscle fibres in the hearts of *TRPV2*$^{flox/flox}$;*MerCreMer*$^{+/-}$ control mice treated only with vehicle, in hearts treated with tamoxifen for 9 days, the contact areas between cells corresponding to intercalated discs were expanded, extended and irregularly shaped (Fig. 2e). Thus, it is possible that the chamber dilation in TRPV2-deficient hearts on day 9 was associated with cellular elongation resulting from the disorganization of the intercalated disc structure. Surprisingly, about 70% of *TRPV2*$^{flox/flox}$;*MerCreMer*$^{+/-}$

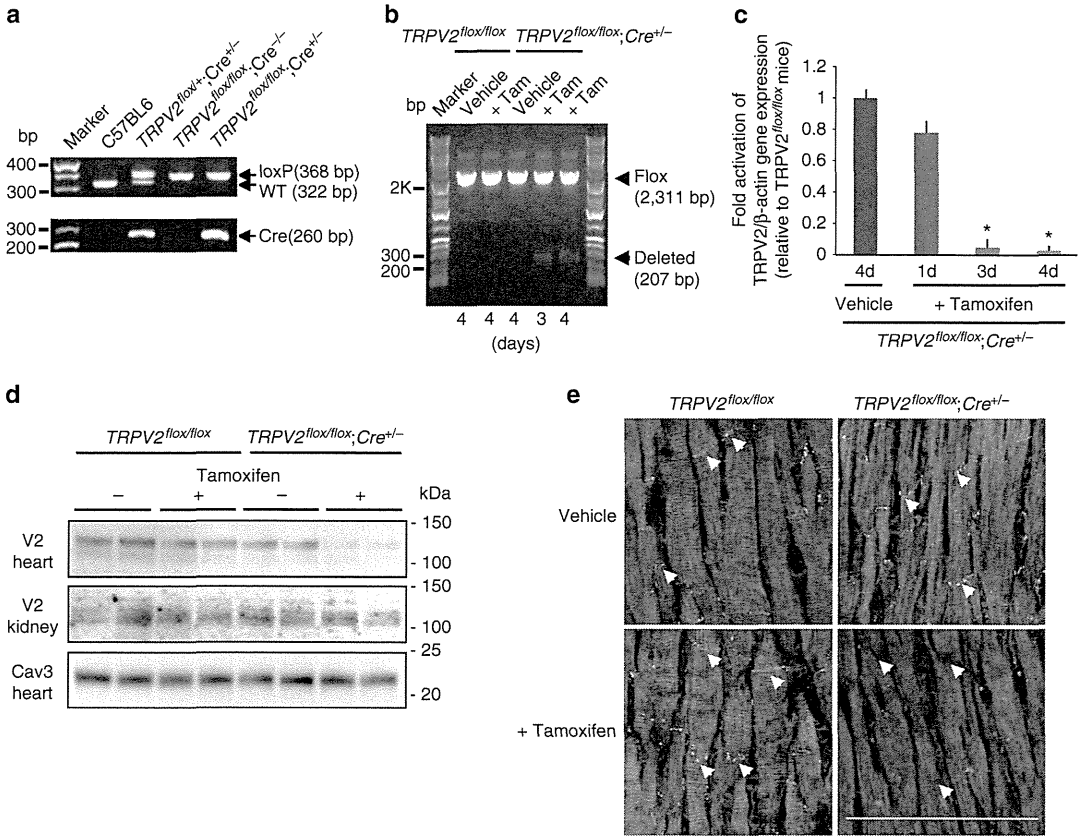

Figure 1 | Generation of temporally controlled cardiac-specific TRPV2-deficient mice. (**a**) Genotyping of *TRPV2*$^{flox/flox}$;*MerCreMer*$^{+/-}$ mice using tail genomic DNA. (**b**) Confirmation of *Cre* recombination by PCR of cardiac genomic DNA. (**c**) TRPV2 messenger RNA expression confirmed by RT-PCR, using β-actin as an internal control gene ($n=3$ mice per group). Data are mean ± s.e.m. *$P<0.05$ versus non-treated age-matched *TRPV2*$^{flox/flox}$; *MerCreMer*$^{-/-}$ (*TRPV2*$^{flox/flox}$) mice. (**d**) Expression of TRPV2 protein in heart and kidney from tamoxifen-treated and -untreated *TRPV2*$^{flox/flox}$ or *TRPV2*$^{flox/flox}$;*MerCreMer*$^{+/-}$ (*TRPV2*$^{flox/flox}$; *Cre*$^{+/-}$) mice, using caveolin 3 as an internal control for hearts. Membrane extracts (10 μg per lane) were subjected to immunoblotting. (See full blots with marker position in Supplementary Fig. 6). (**e**) Triple staining of left ventricle sections with anti-TRPV2 antibody (green), phalloidin (red) and DAPI (blue). Scale bar, 100 μm. Arrows, intercalated discs.

mice died within 10 days of the onset of tamoxifen treatment, suggesting an indispensable role for TRPV2 in the working heart (Fig. 2f).

The cardiovascular function in TRPV2-deficient mice. Echocardiography revealed a severe decline in fractional shortening and an increased left ventricular diastolic dimension 4 days after the start of tamoxifen treatment (Fig. 3a,b). Cardiac dysfunction was not observed in tamoxifen-treated *TRPV2*$^{flox/+}$; *MerCreMer*$^{+/-}$ mice (hetero knockout (KO) mice) for 4 days (Supplementary Fig. 2). Therefore, the cardiac dysfunction seen in TRPV2-deficient mice (homo KO mice) is not due to side effects associated with the overexpression of *Cre* recombinase or tamoxifen administration.

Figure 3c,d show that aortic blood pressure also gradually dropped in TRPV2-deficient mice after 3 days of tamoxifen treatment, although the heart rate did not change (Fig. 3e). Notably, the time course of blood pressure decline closely paralleled the time course of *Cre-loxP* recombination in tamoxifen-treated *TRPV2*$^{flox/flox}$;*MerCreMer*$^{+/-}$ mice (Fig. 1b,c). Therefore, the rapid reduction in blood pressure appeared to result from the severe decline in cardiac pump function following the elimination of TRPV2. This suggests that TRPV2 is critical for cardiac function under basal conditions.

The disordered intercalated discs in TRPV2-deficient hearts. Although the gross morphology of the hearts of tamoxifen-treated *TRPV2*$^{flox/flox}$;*MerCreMer*$^{+/-}$ mice after 4 days was effectively normal (Fig. 2a), the ultrastructure of the intercalated discs was already dramatically disrupted (Fig. 4a), showing extensive interdigitation, irregular shapes, lacunae and widened spaces at the sites of myofibril attachment. Immunostaining for N-cadherin and β-catenin, components of adherens junctions[4–6], showed a denser localization at cell–cell interfaces in TRPV2-deficient hearts compared with vehicle controls (Fig. 4b). The structural abnormality of intercalated disc architecture seen in *TRPV2*$^{flox/flox}$; *MerCreMer*$^{+/-}$ hearts is considered synonymous with impaired mechanical interactions with neighbouring myocytes[15]. These observations suggest that the severe decline in cardiac pump function was associated with the structural disruption of intercalated discs and adherens junctions, suggesting that mechanical coupling at these sites is under the control of TRPV2.

TRPV2 elimination affects myocardial electrical coupling. A number of cardiac disorders have been described in which disruption of the intercalated disc structure significantly affects electrical coupling[4]. In TRPV2-deficient myocytes, 4 days after the onset of tamoxifen treatment, the gap junction protein connexin 43 showed diffuse localization in the intercalated discs

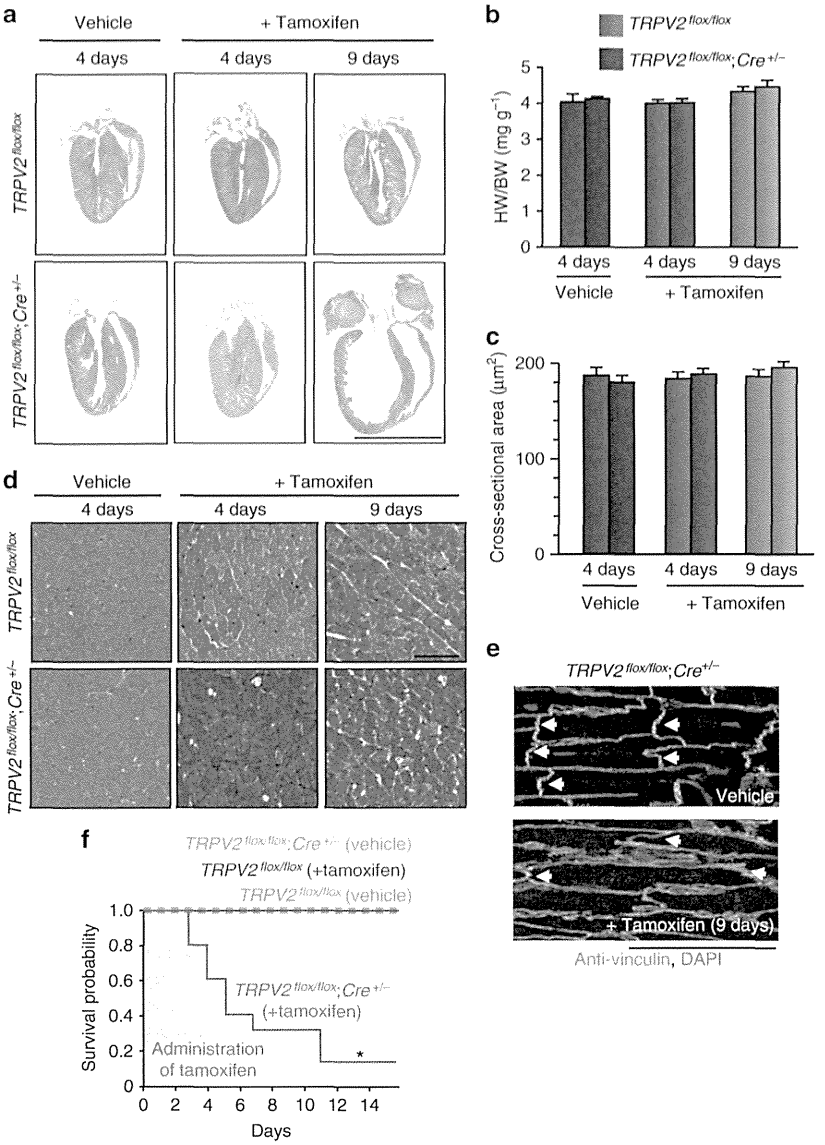

Figure 2 | Morphological changes and survival in TRPV2-deficient mice. *TRPV2*$^{flox/flox}$;*MerCreMer*$^{-/-}$ (*TRPV2*$^{flox/flox}$) and *TRPV2*$^{flox/flox}$;*MerCreMer*$^{+}$ (*TRPV2*$^{flox/flox}$;*Cre*$^{+/-}$) mice, treated with tamoxifen or vehicle, were analysed on day 4 and day 9. (**a**) Cardiac morphology. Scale bar, 5 mm. (**b**) Heart weight (HW)/body weight (BW) ratio. Data are mean ± s.e.m. ($n = 22$–35 hearts per group) (**c**) Cross-sectional areas from paraffin sections of left ventricles. Data are mean ± s.e.m. ($n = 122$–153 cells from three hearts per group) (**d**) Masson's trichrome staining of the left ventricle. Scale bar, 50 μm (**e**) Double staining with anti-vinculin antibody (green) and DAPI (blue). Scale bar, 100 μm. Arrowheads, intercalated discs. (**f**) Survival probabilities ($n = 55$–85 per group). *$P < 0.05$ versus *TRPV2*$^{flox/flox}$;*Cre*$^{+/-}$ mice treated with vehicle, by log-rank tests.

and its expression spread along the sarcolemma over time (Fig. 5a). Typical electrocardiograms obtained by telemetry showed no abnormalities over the first 4 days of tamoxifen administration (Fig. 5b); however, after 5 days, QRS complexes time-dependently widened (Supplementary Fig. 3), and 1 week after the onset of tamoxifen treatment, TRPV2-deficent hearts showed intraventricular conduction delays (Fig. 5b). As this phenomenon occurred several days after a drop in blood pressure was seen (Fig. 3c), it is likely that the disorganization of the intercalated disc architecture after the loss of TRPV2 had an indirect effect on electrical coupling with neighbouring myocytes.

TRPV2-deficient cardiomyocytes are fully functional. Abnormal Ca^{2+} handling by cardiomyocytes is a central cause of contractile dysfunction[3]. To investigate the E–C coupling of TRPV2-deficient myocytes, we analysed contractility and Ca^{2+} handling in single cardiomyocytes from tamoxifen-treated and -untreated *TRPV2*$^{flox/flox}$;*MerCreMer*$^{+/-}$ mice. Despite severe cardiac dysfunction, single myocytes isolated from these mice treated with tamoxifen for 4 days showed no abnormalities in cell morphology and shortening (Fig. 6a,b) or intracellular Ca^{2+} transients evoked by electrical stimulation (Fig. 6c), suggesting that the ablation of TRPV2 causes no significant change in intracellular Ca^{2+} handling for E–C coupling. By contrast, after 9 days of tamoxifen treatment, the isolated TRPV2-deficient cardiomyocytes showed an elongated morphology (Fig. 6a). These myocytes showed significantly impaired contractility (Fig. 6b) and Ca^{2+} cycling (Fig. 6c), compared with vehicle-treated control cells, and electrically evoked Ca^{2+} transient peaks

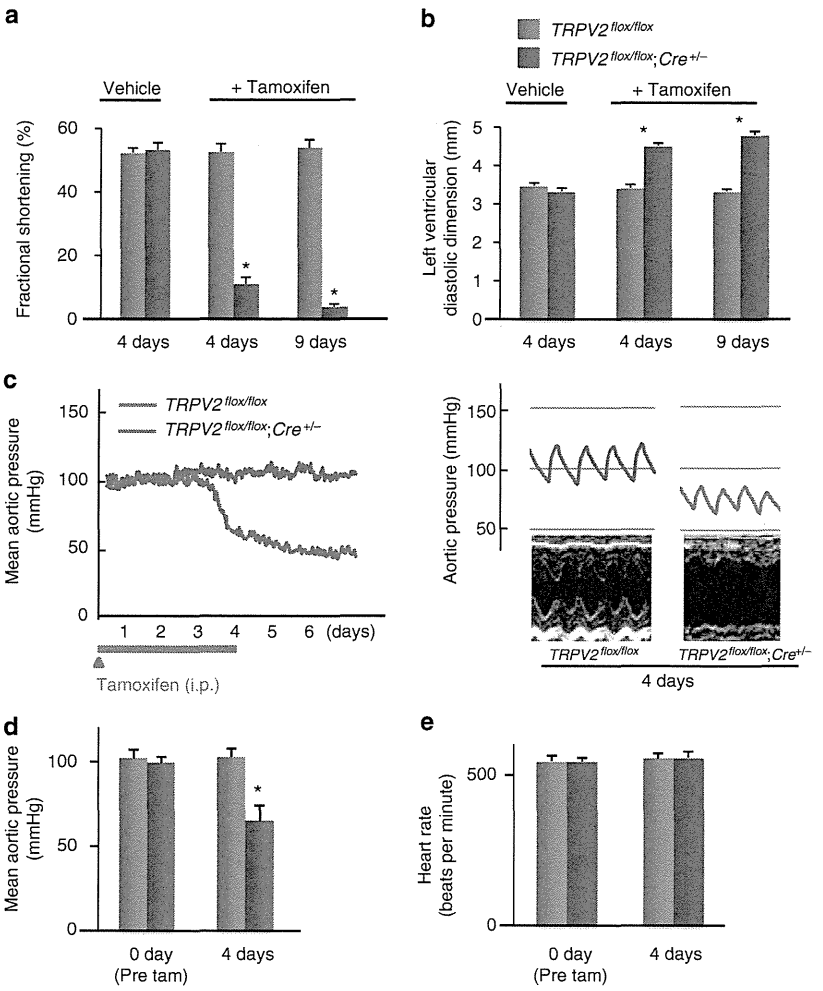

Figure 3 | Rapid, severe decline in cardiac pump function after TRPV2 elimination. (**a**,**b**) Echocardiographic parameters ($n=5$ per group). Data are means ± s.e.m. *$P<0.05$ versus *TRPV2*$^{flox/flox}$;*Cre*$^{+/-}$ mice treated with vehicle, by two-way analysis of variance (ANOVA) with Bonferroni's *post hoc* test. (**c**) Representative pressure recording (left panel), and example of a pressure recording (upper right) and an echocardiograph (lower right) after tamoxifen treatment. (**d**,**e**) Mean aortic pressure and heart rate ($n=3$ per group). Data are means ± s.e.m. *$P<0.05$ versus all other groups, by one-way ANOVA with Bonferroni's *post hoc* test.

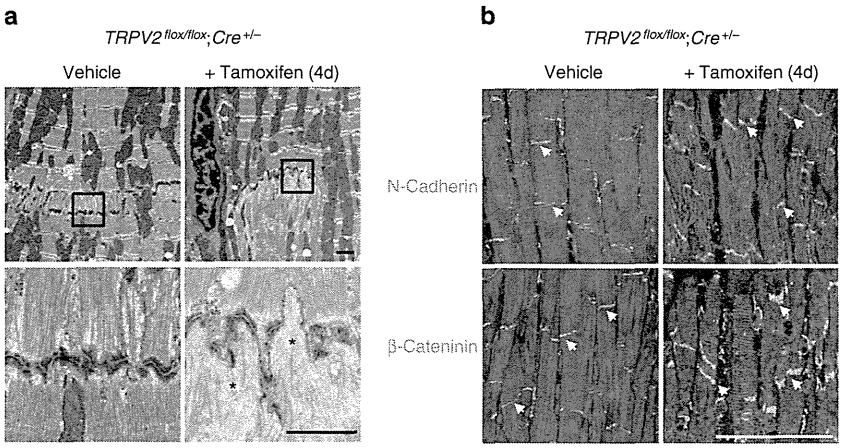

Figure 4 | Disorganization of intercalated discs in TRPV2-deficient hearts. (**a**) Electron micrographs of intercalated discs. Scale bar, 1 μm. Areas in black squares are magnified in lower panels. Asterisks, lacunae in intercalated discs. (**b**) Localization of N-cadherin and β-catenin in tamoxifen-treated *TRPV2*$^{flox/flox}$;*Cre*$^{+/-}$ mouse hearts. Scale bar, 75 μm. Arrows, intercalated discs.

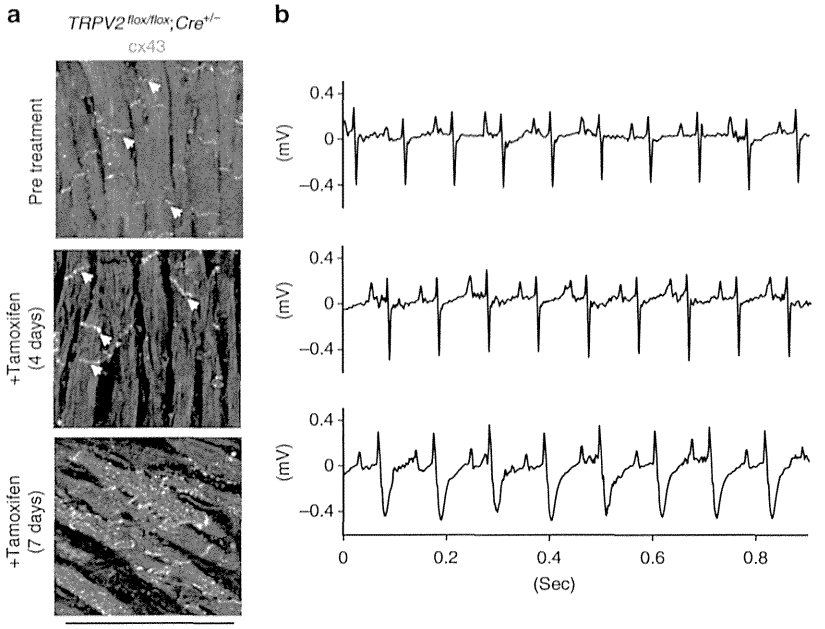

Figure 5 | Cardiac conduction defects after TRPV2 elimination. (**a**) Change in connexin 43 localization in *TRPV2*$^{flox/flox}$;*Cre*$^{+/-}$ hearts after tamoxifen treatment. Scale bar, 100 μm. (**b**) Intraventricular conduction delay after TRPV2 depletion. Electrocardiographs (comparable with lead II) obtained by telemetry.

with reduced amplitude and a slow decay speed (Fig. 6d,e). In addition, the Ca^{2+} content of the myocyte sarcoplasmic reticulum was reduced (Fig. 6f), although intracellular free Ca^{2+} concentrations under basal conditions were in line with the controls.

The subcellular structure of cardiomyocytes and the localization of Ca^{2+} regulatory proteins are well suited to their cellular functions[21]. In cardiomyocytes, Ca^{2+} release for contraction occurs at distinct structures (dyads) along T-tubules, which are critical for efficient E–C coupling[22]. In the dyad space in control vehicle-treated hearts, L-type Ca^{2+} channels and Na^+/Ca^{2+} exchangers were localized in T-tubules, and ryanodine receptors were located on sarcoplasmic reticulum membranes, so that these immunofluorescence signals appeared as well-ordered patterns (Fig. 7a). In *TRPV2*$^{flox/flox}$;*MerCreMer*$^{+/-}$ mice treated with tamoxifen for 4 days, the key Ca^{2+} regulatory proteins in cardiomyocyte E–C coupling (that is, L-type Ca^{2+} channels, ryanodine receptors, and Na^+/Ca^{2+} exchangers) were normally expressed, and localized in T-tubules and sarcoplasmic reticulum membranes, as in vehicle controls, suggesting normal Ca^{2+} handling in the cardiomyocytes (Fig. 7a,b). The myofilament structures were normal in these tamoxifen-treated mice for 4 days (Fig. 7c). Thus, the main cause of the rapid and severe decline in cardiac pump function in TRPV2-deficient hearts was not abnormal Ca^{2+} handling affecting myocyte E–C coupling or disorganization of contractile filaments.

Abnormal Ca^{2+} handling in TRPV2-deficient myocytes. In *TRPV2*$^{flox/flox}$;*MerCreMer*$^{+/-}$ hearts, 9 days after the onset of tamoxifen treatment the subcellular localization of L-type Ca^{2+} channels, ryanodine receptors and Na^+/Ca^{2+} exchangers was abnormal, representing a defect in intracellular Ca^{2+} handling (Fig. 7a), although the levels of expression of these Ca^{2+} regulatory proteins were similar to controls (Fig. 7b). It was possible that T-tubules and dyad structures were disordered in TRPV2-deficient hearts by day 9. In isolated cardiomyocytes at this stage, RyR activity was not only significantly lower (Fig. 6c,d), but the reaction area of Ca^{2+} sparks elicited by electrical stimulation was also reduced and showed subcellular heterogeneity (Supplementary Fig. 4). TRPV2-deficient myocytes on day 9 also showed extensive disorganization of the myofilaments needed to generate force (Fig. 7c). At this later stage, TRPV2-deficient myocytes showed impaired Ca^{2+} handling (Fig. 6b–f and Supplementary Fig. 4) and disorganization of the contractile cytoskeletal apparatus (Fig. 7c). Thus, eliminating TRPV2 not only led to a rapid and severe decline in normal cardiac pump function, but also resulted in a subsequent cellular dysfunction in individual myocytes.

Characterization of TRPV2-deficient neonatal cardiomyocytes. Intra-, inter- and extracellular mechanical forces play vital roles in the differentiation and maturation of cardiomyocytes, both in *in vivo* and *in vitro*[1–3]. In particular, the formation of mature intercalated discs is important during development for directing myofibrogenesis, appropriate Ca^{2+} handling for E–C coupling and differentiation into synchronously beating myocytes[6]. In cultured newborn cardiomyocytes, we were able to follow the formation of intercalated discs and the reorganization of myofibrils with time in myocytes isolated by enzymatic dissociation from neonatal heart tissue[23]. When we examined the formation of intercalated discs in cultured neonatal cardiomyocytes, by staining for the gap junction protein, connexin 43, and N-cadherin (Fig. 8a, upper and middle, first three panels), we observed that the intercalated disc structures at cell–cell interfaces showed many zigzags, sharp turns and a high degree of convolution. In control cardiomyocytes isolated from *TRPV2*$^{flox/flox}$;*MerCreMer*$^{-/-}$ with or without tamoxifen treatment or *TRPV2*$^{flox/flox}$;*MerCreMer*$^{+/-}$ mice cultured without tamoxifen (Fig. 8a, all panels except for right column), we observed well-developed sarcomeres, typical localization of connexin 43 and N-cadherin to intercalated discs at cell–cell interfaces and synchronously beating myocytes. In these

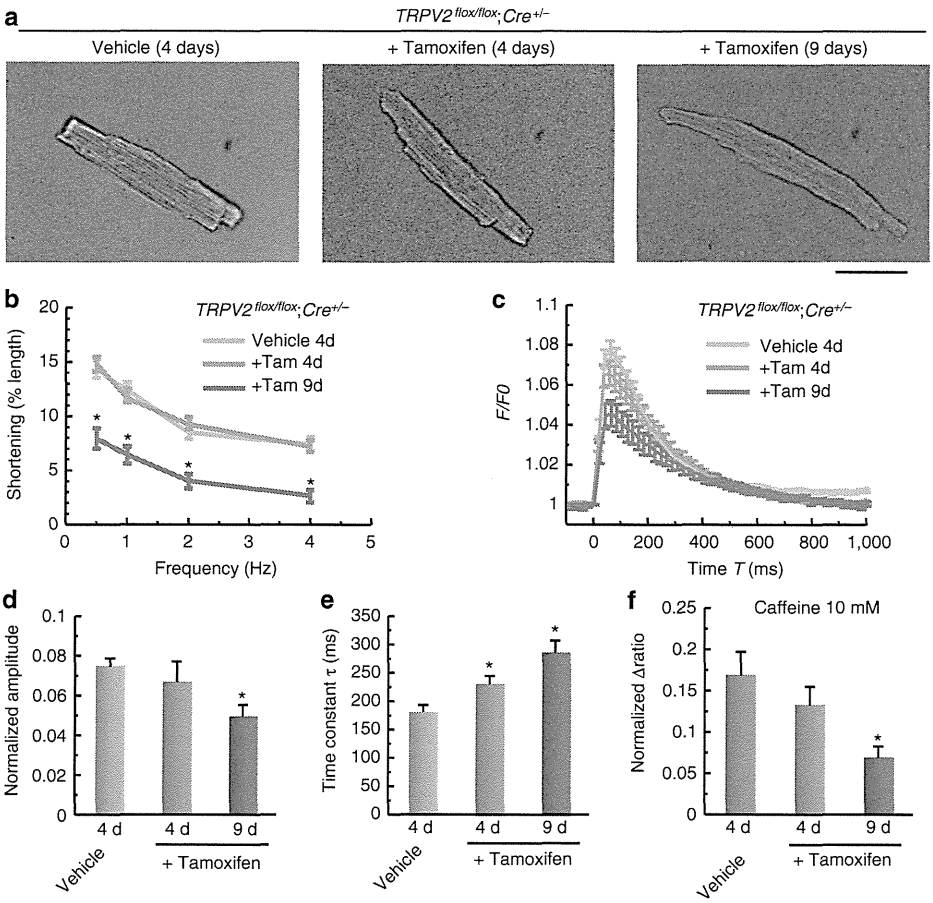

Figure 6 | Cardiomyocyte contractility and Ca^{2+} handling by isolated cells from TRPV2-deficient hearts. (**a**) Morphology of isolated cardiomyocytes. Scale bar, 50 μm. (**b**) Frequency-dependent shortening of myocytes ($n = 100$, 175, and 58 cells measured from 8, 6 and 3 hearts). (**c**) Indo-1 fluorescence in single cardiomyocytes stimulated at 1 Hz ($n = 28$, 18 and 12 cells from 7, 4 and 3 hearts). (**d**) Peak amplitude of Ca^{2+} transients. (**e**) Decay time constant obtained by fitting the decline phase. (**f**) Estimation of sarcoplasmic reticulum Ca^{2+} content. Data are means ± s.e.m. $^*P < 0.05$ versus vehicle control.

cardiomyocytes, NCX1 was highly expressed at the cell surface and at intercalated areas, indicating their maturation and differentiation into synchronously beating myocytes (Fig. 8a, first three bottom panels). By contrast, TRPV2-deficient myocytes cultured with 0.2 μg ml^{-1} tamoxifen for 48 h formed no intercalated discs between neighbouring cells, and showed aberrant intracytoplasmic accumulation of connexin 43, internally defuse N-cadherin, and reduced expression of NCX1 (Fig. 8a, right panels). Although we observed spontaneous weak beating in TRPV2-deficient myocytes, it was not synchronous.

Previously, we reported that recombinant TRPV2 in Chinese hamster ovary cells could be activated by stretch-induced mechanical stimulation[17,18]. We investigated whether neonatal cardiomyocytes showed an intracellular Ca^{2+} increase after stretch stimulation dependent upon TRPV2. In *TRPV2$^{flox/flox}$;MerCreMer$^{+/-}$* myocytes untreated with tamoxifen, an extracellular Ca^{2+}-dependent intracellular Ca^{2+} increase was detected after stretch stimulation, which was blocked by inhibitors of stretch-activated channels, Gd^{3+} or ruthenium red (RR) (Fig. 8b–d). Although RR is known to block RyR, its effect is not permanent, so using a bath application should limit its effects to plasma membrane channels[24]. By contrast, no stretch-evoked Ca^{2+} increase was observed in tamoxifen-treated myocytes. In addition, we confirmed the stretch-evoked Ca^{2+} increase in HEK293 cells expressing TRPV2 and the blockade of this response by Gd^{3+} or RR (Fig. 8e). These results indicate that TRPV2 is a key molecule in the stretch-induced Ca^{2+} response of cardiomyocytes. Interestingly, the formation of intercalated discs and the maturation into cardiomyocytes showing the synchronized beating and alignment of myofilaments seen in vehicle-treated *TRPV2$^{flox/flox}$;MerCreMer$^{+/-}$* myocytes were disturbed in the presence of RR at the same level as in TRPV2-deficient myocytes (Fig. 8f). Taken together, these findings suggest that TRPV2 activation is required for the formation of intercalated discs connecting neighbouring myocytes and their maturation into synchronously beating myocytes.

Stretch-dependent TRPV2 activation controls IGF-1 secretion. Substantial evidence from genetic mouse models has demonstrated the critical role of the IGF-1 receptor/PI3K/Akt pathway in maintaining physiological cardiac morphology and function[25]. Surprisingly, the connection with neighbouring myocytes and sarcomere orientation was maintained in TRPV2-deficient myocytes, when IGF-1 was added to cultures (Fig. 9a). Therefore, we measured IGF-1 secretion from cardiomyocytes in culture in response to cyclic stretch stimulation at 1 Hz for 30 min. IGF-1 secretion was markedly elevated in control

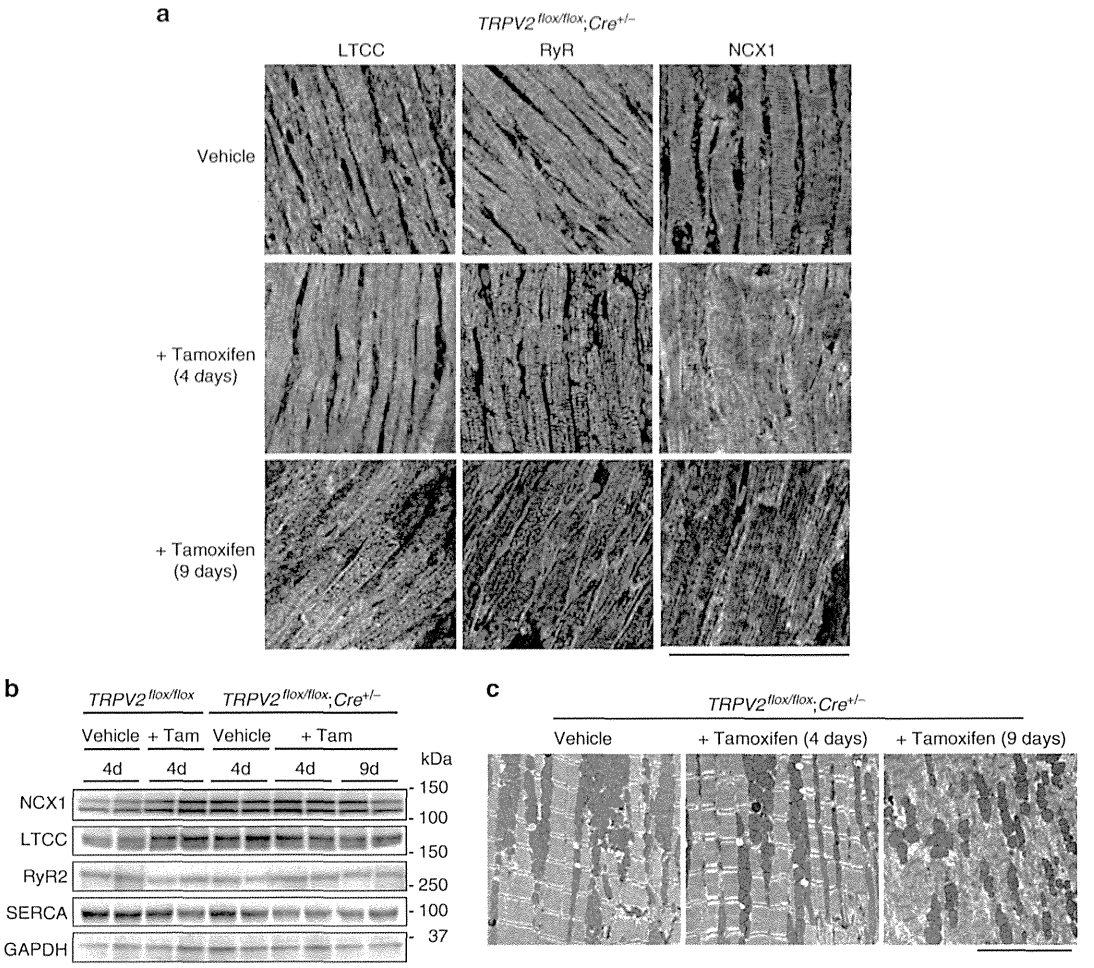

Figure 7 | Expression of Ca^{2+} handling protein by isolated cardiomyocytes and electron micrographs of myofibrils in TRPV2-deficient hearts. (**a**) Time-dependent changes in the localization of the Ca^{2+} regulatory proteins LTCC, RyR and NCX1 in tamoxifen-treated *TRPV2*$^{flox/flox}$;*Cre*$^{+/-}$ mice. Double staining with anti-LTCC antibody (green) and DAPI (blue) in cardiac muscle (left panels). Double staining with anti-RyR antibody (green) and DAPI (blue) in cardiac muscle (middle panels). Double staining with anti-NCX1 antibody (green) and DAPI (blue) in cardiomyocytes (right panels). Scale bar, 100 μm. (**b**) Expression of NCX1, LTCC, RyR and SERCA proteins in TRPV2-deficient heart extracts (10 μg per lane), using GAPDH as the internal control in cardiac muscle, (see full blots in Supplementary Fig. 6). (**c**) Electron micrographs of myofibrils in cardiomyocytes from *TRPV2*$^{flox/flox}$;*Cre*$^{+/-}$ mice, untreated or treated with tamoxifen. Scale bar, 5 μm.

myocytes and was blocked by the inhibitors of stretch-activated channels, Gd^{3+} or RR, whereas it was significantly reduced in TRPV2-deficient myocytes (Fig. 9b).

IGF-1 secreted from cardiomyocytes and fibroblast promotes the cardioprotective response to severe pressure overload by activating PI3K and its downstream effector Akt[26,27]. Patients with heart failure have been reported to have significantly lower IGF-1 levels compared with controls[28]. In *TRPV2*$^{flox/flox}$;*MerCreMer*$^{+/-}$ mice treated with tamoxifen for 3 or 4 days, *IGF-1*, *IGF-1 receptor*, *PI3Kα* and *Akt1* expression was significantly reduced (Fig. 9c–f). These observations suggest that the IGF-1 receptor/PI3K/Akt pathway is downregulated in TRPV2-deficient hearts.

Effects of IGF-1 administration in TRPV2-deficient hearts. To investigate whether the reduced IGF-1 signalling seen in TRPV2-deficient mice represented a significant molecular basis for their observed heart failure phenotype, we treated TRPV2-deficient mice with recombinant IGF-1. In normal mice, IGF-1 administration for 1 week resulted in an increase in cardiac mass and heart-to-body weight ratio (Fig. 9g,h). Remarkably, in TRPV2-deficient mice, administering IGF-1 prevented both the enlargement of the left ventricular diastolic dimensions and cardiac dysfunction (Fig. 9i,j). In addition, expression of *IGF-1 receptor*, *PI3Kα* and *Akt1* were all significantly increased by the administration of IGF-1 in TRPV2-deficient hearts (Supplementary Fig. 5). These results suggest that reduced IGF-1 signalling is a major factor in the heart failure observed in TRPV2-deficient mice. However, IGF-1 administration did not result in complete recovery, suggesting that other signalling pathways may also be impaired in TRPV2-deficient hearts.

Discussion

This study has shown a critical role for TRPV2 in the normal heart. TRPV2 is localized at intercalated discs, which are critical for detecting the mechanical forces generated by myocyte contraction. The elimination of TRPV2 from the mouse heart resulted in severe cardiac dysfunction within a few days (Fig. 3),

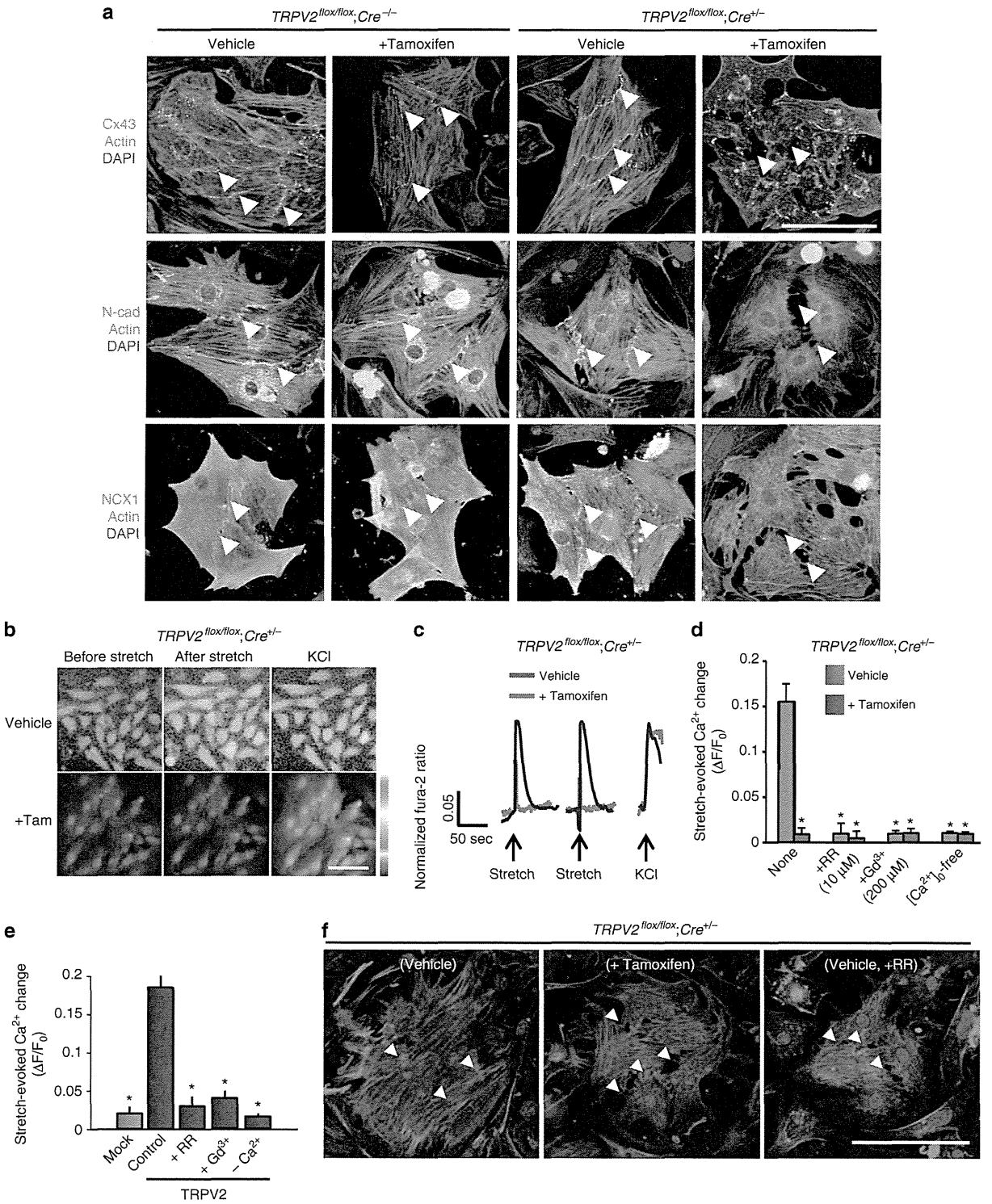

Figure 8 | Impairment of maturation into functional syncytia with synchronously beating cardiomyocytes in TRPV2-deficent newborn mice. (**a**) Isolated cardiomyocytes from *TRPV2*$^{flox/flox}$;*Cre*$^{-/-}$ or *TRPV2*$^{flox/flox}$;*Cre*$^{+/-}$ newborn mice. Triple staining with anti-connexin 43 antibody (green), phalloidin (red) and DAPI (blue) in cardiomyocytes (upper panels). Triple staining with anti-N-cadherin antibody (green), phalloidin (red) and DAPI (blue) in cardiomyocytes (middle panels). Triple staining with anti-NCX1 antibody (green), phalloidin (red) and DAPI (blue) in cardiomyocytes (lower panels). Scale bar, 100 μm. (**b**) Fura-2-imaging of stretch-induced intracellular Ca^{2+} dynamics in neonatal cardiomyocytes. Scale bar, 100 μm. (**c**) Representative trace of stretch-induced intracellular Ca^{2+} increase. (**d**) Effect of mechanosensitive channel inhibitors. Data are means ± s.e.m. *$P<0.01$ versus vehicle control ($n=19$–44). (**e**) Stretch-induced Ca^{2+} changes in ectopically expressed TRPV2 in HEK293 cells. Data are means ± s.e.m. *$P<0.01$ versus control. ($n=23$–37) (**f**) Isolated cardiomyocytes from newborn mice cultured with 10 μM rubidium red. Scale bar, 100 μm. Arrowheads, cell-cell junctions.

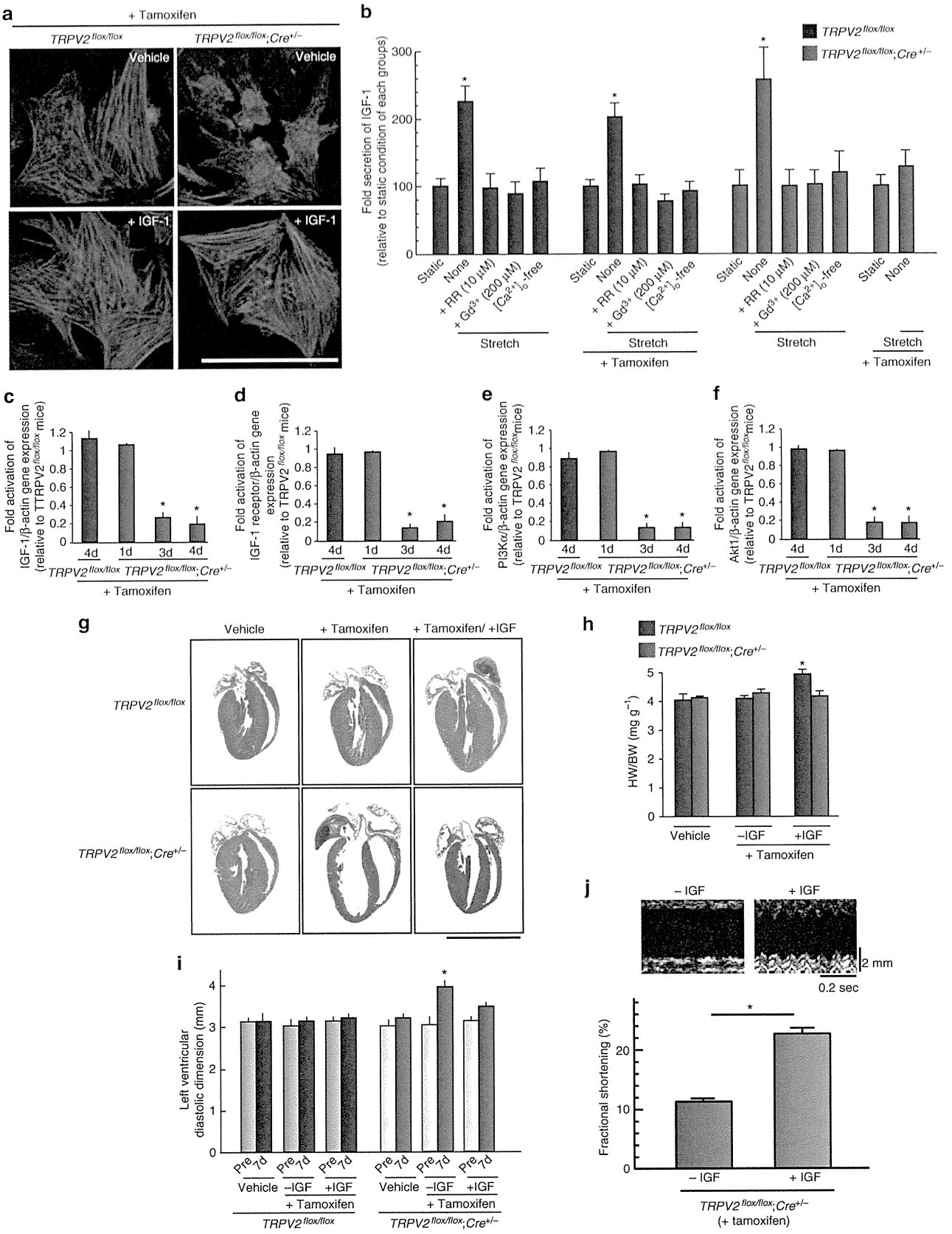

despite no impairment of myocyte contraction or E–C coupling efficiency (Fig. 6). These observations suggest that the functional integration with neighbouring cardiomyocytes was weakened in TRPV2-deficient hearts. It seems that cardiomyocytes sense inadequate functional output at a cellular level and respond by increasing the number of myofibrillar attachment sites in intercalated area[7]. In a failing heart, the elevated expression of adherens junction proteins and the increase in membrane convolution and interdigitation between neighbouring cardiomyocytes seems to lead to a decrease in the flexibility of the contractile tissue and increased stiffness[7]. In TRPV2-deficient hearts, the myofilaments were disassembled at their attachment sites to intercalated discs (Fig. 4a). The TRPV2-deficient myocytes did not seem to sense the inadequate functional output or the severe cardiac dysfunction and therefore might have difficulty maintaining the integrity of their intercalated discs. On the other hand, cultured neonatal cardiomyocytes from TRPV2-deficient mice showed impaired formation of intercalated discs and translocation of connexin 43 and N-cadherin into cell–cell adhesion sites, and no spontaneous, synchronized beating (Fig. 8a). The TRPV2 inhibitor, RR, also affected intercalated disc formation in neonatal cardiomyocytes (Fig. 8f), implicating TRPV2 activity in the maintenance of intercalated disc integrity as well as their formation. Further experiments are needed to elucidate the molecular mechanism involved in maintaining intercalated disc structure and exactly how this function depends upon TRPV2.

It is possible that TRPV2 has a pivotal role as an anchoring protein for myofibrils at intercalated discs, coordinating the transmission of mechanical forces regardless of its channel activity. The transmission of the force generated by contracting myofibrils is mediated by so-called adherens junctions, which are composed of transmembrane proteins of the cadherin family and which, in the cytoplasm, are coupled to the contracting sarcomeres by members of the catenin family[7]. Reportedly, TRPV4 associates with adherens junctions via α-catenin in the human bladder urothelium[29]. In common with several members of other TRP subfamilies[30], the cytoplasmic region of TRPV2 is likely to couple to a rigid intracellular structural network and form 'mechanosensitive Ca^{2+}-signalosomes' at intercalated discs. If so, eliminating TRPV2 is therefore likely to interrupt mechanical coupling with neighbouring myocytes at intercalated discs, causing severe cardiac dysfunction.

In addition, we showed a significant reduction of stretch-dependent IGF-1 secretion in TRPV2-deficient myocytes (Fig. 9b), and a downregulation of IGF-1 receptor/PI3K/Akt signalling in TRPV2-deficient hearts (Fig. 9c–f). IGF-1 is continuously secreted in the normal state and in response to mechanical stress dependent on the intracellular Ca^{2+} concentration[25,26,31]; this in turn modulates myocyte PI3K signalling, which is involved in myocardial hypertrophy and heart failure[25]. It appears that the TRPV2 activation-dependent IGF-1 secretion of cardiomyocytes controls the equilibrium balance of intracellular IGF-1 receptor/PI3K/Akt signalling in response to haemodynamic stress. This forms a molecular basis for the myocyte mechanical feedback mechanism in the normal state and in response to haemodynamic stress, which is required to maintain cardiac structure and function. Therefore, loss of TRPV2 not only leads to a rapid and severe decline in normal cardiac pump function, but also triggers subsequent cellular dysfunction in individual myocytes.

TRP channels are unique cellular sensors responding to a wide variety of extracellular and intracellular signals, including mechanical and osmotic stress[32]. The present study shows that TRPV2 is a candidate molecule for stretch-activated channels in myocyte intercalated discs, and is crucial for the mechanical stimulation-dependent Ca^{2+} signalling of cardiomyocytes. However, it is unclear whether TRPV2 channels directly transduce mechanical stimuli or are part of a downstream signalling pathway, as discussed below. Several regulatory interactions between TRPV2 cytoplasmic domains and various signalling molecules have been investigated. Mercado *et al.*[33] proposed that PIP_2 is constitutively associated with the C-terminal domain of TRPV2, promoting its inhibition Ca^{2+}-dependently. It is not yet certain that TRPV2 directly senses membrane lipid stretching through PIP_2 breakdown and diacylglycerol production, as has been shown for other mechanosensitive channels[34,35]. Therefore, to clarify the regulatory mechanism of TRPV2 activation, further electrophysiological investigations will be needed in the future.

TRPV2 has been reported to translocate from an intracellular compartment to the plasma membrane in response to IGF-1 and intracellular Ca^{2+} concentration[17,36]. Therefore, the appropriate control of these mediators might be needed for the localization of TRPV2 to the membrane in intercalated discs in working hearts. It is possible that the transmission and generation of mechanical force during contraction in response to haemodynamic stress provides the control for IGF-1 production and intracellular Ca^{2+} concentrations, in which TRPV2 plays a pivotal role by continuously monitoring mechanical stress. TRPV2 activity is also directly controlled by PI3K activity, and this is independent of channel translocation to the plasma membrane[37]. Activation of PI3K by growth factors results in PIP_3 synthesis, by the phosphorylation of PIP_2 (ref. 25). Thus, TRPV2 activity is also likely to be regulated by the PIP_2 content, dependent on PI3K activity, and interactions with other lipids in intercalated discs. However, little is known about the lipid composition of intercalated discs. Taken together, these findings suggest that the lipid composition and potentiation of the IGF-1 receptor/PI3K/Akt signalling cascade in response to haemodynamic stress are key factors for TRPV2 activation at intercalated discs in the heart.

This study has identified a molecular basis for the maintenance of cardiac structure and function, through myocyte mechanical feedback systems, in which TRPV2 plays a pivotal role (Fig. 10). The integrity of intercalated discs has a large impact on force transmission and generation during muscle contraction, and is reflected in the effect of mechanical feedback on the quality of myocytes in the heart. Eliminating TRPV2 had no effect on Ca^{2+} handling in myocyte E–C coupling (Fig. 6b–f), which is generated at dyads formed between a T-tubule and the junctional part of the sarcoplasmic reticulum. It appears that the Ca^{2+} signalling

Figure 9 | Impairment of stretch-dependent IGF-1 secretion and IGF-1 receptor/PI3K/Akt pathway in TRPV2-deficient yocytes. (**a**) Isolated cardiomyocytes from newborn mice cultured with 10 μM IGF-1. Scale bar, 100 μm. (**b**) Stretch-dependent IGF-1 secretion by cardiomyocytes. $^*P<0.05$ versus the other groups. Data are means ± s.e.m. (**c–f**) *IGF-1, IGF-1 receptor, PI3Kα and Akt* expression level in TRPV2-deficient hearts ($n=3$ mice per group). $^*P<0.05$ versus non-treated $TRPV2^{flox/flox}$ mice. Data are means ± s.e.m. (**g**) Histological analysis 7 days after onset of IGF-1 administration and tamoxifen treatment in TRPV2-deficient mice. Scale bar, 5 mm. (**h**) HW/BW ratio. Data are means ± s.e.m. ($n=5$–12 per group) $^*P<0.05$ for tamoxifen-treated $TRPV2^{flox/flox};Cre^{+/-}$ mice versus IGF-1-treated $TRPV2^{flox/flox};Cre^{+/-}$ mice after 7 days. (**i,j**) Echocardiographic parameters ($n=3$ per group). (**i**) Data are means ± s.e.m. $^*P<0.05$ versus all the other groups. by two-way analysis of variance with Bonferroni's *post hoc* test.

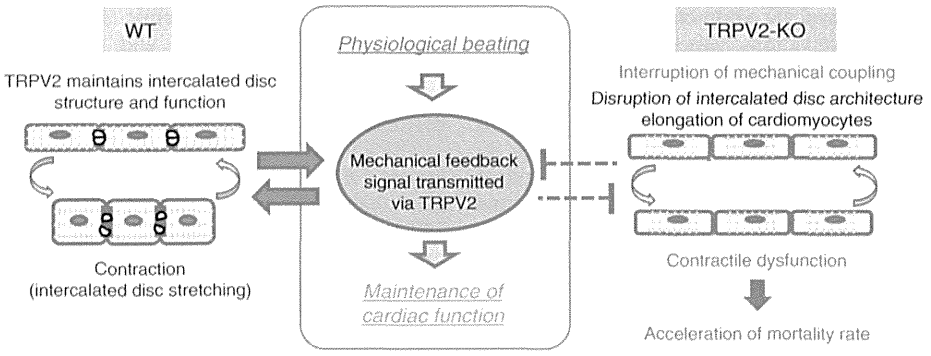

Figure 10 | Role of TRPV2 within the working heart. *In wild-type mice, TRPV2 protein (yellow) is located in the intercalated discs (red), which is cyclically* stretched and accompanied by cardiac contractions within the working heart. The mechanical feedback signal transmitted via TRPV2 is crucial for the maintenance of cardiomyocytes. TRPV2 ablation leads to the disruption of the intercalated disc architecture (red), and disorganization of sarcomere myofibril proteins at the intercalated discs (orange). These TRPV2-KO myocytes show contractile dysfunction. Therefore, the mortality rate of TRPV2-KO mice is accelerated. Thus, the mechanical feedback signal within the working heart integrates myocyte structure and function, with TRPV2 playing a pivotal role.

involved in myocyte E–C coupling and the mechanical signal mediated by TRPV2 are spatially and temporally controlled by different signals in cardiomyocytes. Further studies might clarify the molecular mechanism of mechanotransduction mediated by TRPV2 in cardiomyocytes, and so improve our understanding of cardiac development and maturation, hypertrophic remodelling in the heart and the pathophysiology of heart disease.

Recently, Rubinstein *et al.*[38] reported the cardiac function of TRPV2-KO mice expressing *Cre* under the control of the cytomegalovirus promoter generated by Park *et al*[39]. They observed that cardiac function declined in TRPV2-deficient mice compared with controls, despite no histological abnormality[38]. Although there are differences in the severity of cardiac dysfunction and the depression of myocyte contractility, these results are consistent with our observations. However, the construction of their TRPV2-KO mice differed from our model in the site at which the partial elimination occurred, which corresponded to the channel pore and carboxy-terminal region of TRPV2, using a ubiquitous promoter, and the genetic background of the mice (B6129SF2/J)[39]. Park *et al.*[39] have reported that their model was susceptible to perinatal lethality but displayed normal thermal and mechanical nociception. They therefore suggested the possibility that compensatory mechanisms prevented the obvious phenotype of TRPV2-deficient cells being reflected in their KO mice[39]. On the other hand, the cardiac-specific elimination of TRPV2 in this study affected neither the embryonic development nor the growth after birth, in the absence of tamoxifen administration. Taken together, we believe that the acute elimination of TRPV2 function in our model might circumvent any hypothetical compensatory process.

Methods

Animals. Mice were housed under a 12-h light–dark cycle in a temperature-controlled environment. All the experiments were performed in male mice aged 10 weeks old (weighing 22–24 g). Littermates were used in this study to randomize genetic variation. All animal experiments were approved by the Animal Research Committee of Okayama University (Okayama, Japan), and were performed in accordance with institutional guidelines.

Generation of TRPV2 conditional KO mice. All experiments requiring gene recombination in this study were carried out in accordance with the institutional guideline of Okayama University (Okayama, Japan). Using cloned TRPV2 cDNA (accession code. NM011706) as a probe, we screened a genomic library constructed from C57/BL6J mouse DNA. The genomic clone was used to generate the targeting vector shown in Supplementary Fig. 1, which was linearized for electroporation into C57/BL6J ES cells. After selection, G418-resistant ES clones were screened for the presence of the targeted locus by southern blot analysis. Targeted ES cells were microinjected into Balb/c mouse blastocysts, and germline transmission of the TRPV2 conditional null alleles was confirmed by southern blotting and PCR genotyping using genomic DNA extracted from mouse tail veins. We crossed mice carrying a $TRPV2^{flox}$ allele with transgenic mice (*MerCreMer*) expressing tamoxifen-inducible cardiomyocyte-specific Cre recombinase to produce $TRPV2^{flox/flox}$;$MerCreMer^{+/-}$ mice. Germline transmission of TRPV2 conditional null alleles was confirmed by southern blotting and PCR genotyping using the primer pair 5′-TTAAATGACTTGTGAGGGAGATAGC-3′ and 5′-CAAGTAACA CAATCTACCCAAGGTC-3′, yielding 322 (wild-type) and 369 (null allele) bp products. To induce *Cre*-mediated recombination, we injected 10-week-old male $TRPV2^{flox/flox}$;$MerCreMer^{+/-}$, $TRPV2^{flox/+}$;$MerCreMer^{+/-}$ and $TRPV2^{flox/flox}$;$MerCreMer^{-/-}$ mice intraperitoneally with 8 mg kg^{-1} tamoxifen (Sigma) once daily for 4 consecutive days. Tamoxifen injection and subsequent analyses were performed in a blinded fashion.

Electrocardiography. Transthoracic electrocardiography (ECG) was used to evaluate cardiac function with the Aplio 300 (Toshiba Medical System) and a 14-MHz transducer. The 10-week-old male mice were anesthetized initially with 2% isoflurane, and then at 1% during the examination. Left ventricular short-axis dimensions at the tip of the papillary muscles were measured on M-mode. Fractional shortening was calculated as (LVDd–LVDs)/LVDd × 100 (%).

Blood pressure measurement. Chronic measurements of blood pressure and ECG were performed on unrestrained, conscious mice (10-week-old, male) using a commercially available telemetry and computer-based data acquisition system (Data Sciences International) according to the manufacturer's instructions. Briefly, a pressure-sensing catheter was implanted in the thoracic aorta via the left carotid artery, and two electrodes were placed subcutaneously on the right shoulder and left inguinal region to record lead II ECG under anaesthesia with 2% isoflurane inhalation. Mice were returned to their home cage (placed on top of telemetry receivers), and blood pressure and ECG were continuously monitored and recorded.

Administration of IGF-1. Recombinant human IGF-1 was purchased from Cell Science, and diluted with 0.9% NaCl at a concentration of 10 mg ml^{-1} and administered to mice (60 μg per day) by continuous infusion (0.25 μl h^{-1}) using a mini osmotic pump (Alzert 1002). IGF-1 administration and tamoxifen treatment were started at the same time. Control mice received vehicle alone.

Neonatal cardiomyocyte culture. Primary cardiomyocyte cultures were prepared from ventricles of 1-day-old mice by very gentle trypsinization at room temperature, by a modification of preparation methods from rat neonatal heats[40]. Hearts were rapidly removed from neonatal $TRPV2^{flox/flox}$;$MerCreMer^{+/-}$ or $TRPV2^{flox/flox}$;$MerCreMer^{-/-}$ mice anesthetized with an overdose of diethyl ether. The ventricles were excised, cut into several pieces and washed three times with 10 ml ice-cold phosphate-buffered saline for 1 min by gentle shaking. The tissue pieces were digested three times with 0.06% trypsin in DMEM (8 ml) for 8 min at 37 °C by gentle agitation. The cell suspension was resuspended in DMEM with 10% fetal calf

serum (FCS) to stop trypsinization, and was centrifuged at 14*g* for 3 min. The cell pellets were resuspended in fresh DMEM containing 10% FCS, and plated on collagen-coated 24-well dishes at a density of 4×10^4 cells per well and maintained in DMEM containing 10% FCS. The formation of myocytes clusters and the spontaneous synchronized beating were confirmed by inverted microscope (CKX41, Olympus).

Stretch stimulation of cardiomyocytes. For stretch stimulation of cardiomyocytes, the cell suspension were plated on 1 cm^2 collagen-coated polydimethylsiloxane stretch chambers at 2×10^5 cells per well, and cultured. After 24 h, primary cardiomyocytes were divided into two groups and maintained for up to 2 days in DMEM containing 10% FCS, with or without tamoxifen (0.2 μM ml^{-1}). Membranes were uniformly stretched by 20% for 3 s, using a computer-controlled stepping motor machine (STB-150, STREX), by a slight modification of cell-stretch culture methods[41]. One end of the chamber was firmly attached to a fixed frame, while the other was attached to a movable frame connected to a motor-driven shaft. The amplitude and frequency of stretch were controlled by a programmable microcomputer. The silicon membrane was uniformly stretched over the whole membrane area, and the lateral thinning did not exceed 1% at 20% stretch. TRPV2 deficiency did not have a discernible impact on the cardiomyocytes' ability to adhere to the membrane, although the cell–cell interfaces with neighbouring myocytes were expanded.

Stretch-induced Ca^{2+}-transients in newborn cardiomyocytes. Stretch-induced Ca^{2+} transients were examined in cardiomyocytes loaded with 2 μM fura-2 acetoxymethyl ester (fura-2) for 30 min at 37 °C and maintained in standard Tyrode's solution under continuous flow using a microperfusion system. Fura-2-loaded cells were alternately excited at 340 and 380 nm using a Lambda DG-4 Ultra High Speed Wavelength Switcher (Sutter Instruments) coupled to an inverted IX71 microscope with a UApo 20 × /0.75 objective lens (Olympus). Fura-2 fluorescent signals were recorded (ORCA-Flash 2.8; Hamamatsu Photonics) and analysed by a ratiometric fluorescence method using MetaFluor software (version 7.7.5.0; Molecular Devices).

Isolation of adult mouse ventricular myocytes. Ventricular myocytes were obtained from 10-week-old male *TRPV2$^{flox/flox}$;MerCreMer$^{+/-}$* and *TRPV2$^{flox/flox}$;MerCreMer$^{-/-}$* mice by a slight modification of Shioya's methods[42]. Hearts were rapidly removed from adult *TRPV2$^{flox/flox}$;MerCreMer$^{+/-}$* or *TRPV2$^{flox/flox}$;MerCreMer$^{-/-}$* mice anesthetized with an overdose of pentobarbital (300 mg kg^{-1}, intraperitoneally), and Langendorff perfused at a constant hydrostatic pressure of 70 cm H_2O at 37 °C using cell isolation buffer (CIB) supplemented with 0.4 mM EGTA (EGTA–CIB), which chelates calcium within the heart. CIB contained 130 mM NaCl, 5.4 mM KCl, 0.5 mM $MgCl_2$, 0.33 mM NaH_2PO_4, 22 mM glucose, 50 nM ml^{-1} bovine insulin (Sigma) and 25 HEPES-NaOH (pH = 7.4). Insulin was used from 1 U ml^{-1} stock solution in 0.1 mM HCl (pH = 4.0). EGTA was from 400 mM stock in 1 M NaOH (pH = 7.8). The perfusate was then switched to the enzyme solution (15 ml), which was CIB supplemented with 0.3 mM $CaCl_2$, 1 mg ml^{-1} collagenase (Worthington Biochemical), 0.06 mg ml^{-1} trypsin (Sigma) and 0.06 mg ml^{-1} protease (Sigma). Once the tissue had undergone complete digestion, the ventricles were excised, cut into several pieces and further digested in fresh enzyme solution (15 ml) for 15–20 min at 37 °C until they were mostly dissociated. In this enzyme solution, the $CaCl_2$ level was increased to 0.7 mM, and 2 mg ml^{-1} BSA (Sigma) was supplemented. The cell suspension was centrifuged at 14*g* for 3 min. The cell pellet (~0.1 ml) was resuspended in CIB supplemented with 1.2 mM $CaCl_2$ and 2 mg ml^{-1} BSA, and then incubated at 37 °C for 10 min, centrifuged (14*g*, 3 min) and resuspended in 10 ml Tyroad solution supplemented with 2 mg ml^{-1} BSA. Tyrode's solution contained 140 mM NaCl, 5.4 mM KCl, 1.8 mM $CaCl_2$, 0.5 mM $MgCl_2$, 0.33 mM NaH_2PO_4, 11 mM glucose and 5 mM HEPES-NaOH (pH = 7.4)[40,42].

Cell shortening and Ca^{2+} transients in adult cardiomyocytes. Isolated cardiomyocytes were loaded with 10 μmol l^{-1} Indo-1 AM (Invitrogen) and electrically stimulated at 1 Hz using a two-platinum electrode insert connected to a bipolar stimulator (Nihon Kohden, SEN-3301) on the stage of an inverted microscope (IX71, Olympus) with a × 20 water immersion objective lens (UApo N340, Olympus). Calcium transients were measured as the ratio of fluorescence emitted at 405/480 nm after excitation at 340 nm using a high-performance Evolve EMCCD camera (Photometrics). Cardiomyocytes were maintained under continuous flow in standard Tyrode's solution, exchanged using a microperfusion system. For measuring caffeine-induced calcium transients, cells were paced at 1 Hz prior to induction of caffeine contractures. Electrical stimulation was stopped 15 s before rapid perfusion with a 10 mmol l^{-1} caffeine solution. The experiments were recorded and analysed using MetaMorph software (version 7.7.1.0; Molecular Devices). Results were the means of the fluorescent signals from 10–20 cardiomyocytes from a single heart.

Measure of IGF-1 concentration. IGF-1 concentrations were measured in conditioned media from stretched and unstretched myocytes in a sandwich ELISA using mouse standards, according to the manufacturer's guidelines (R&D Systems), which quotes the sensitivity of this assay as 30 ng ml^{-1}. Standard curves and positive controls were included in each assay, and IGF-1 concentrations were obtained by interpolation.

Real-time PCR. The Mouse PI3K-AKT Signalling Pathway RT^2 Profiler PCR Array was purchased from Qiagen. Total RNA extracted from *TRPV2$^{flox/flox}$;MerCreMer$^{+/-}$* or *TRPV2$^{flox/flox}$;MerCreMer$^{-/-}$* hearts with or without tamoxifen were reverse transcribed into cDNA with oligo (dT) primers using Superpscript III. Real-time PCR was performed with Step-One plus^{TM} (Applied Biosystem). Statistical analysis of the results was performed with the $^{\Delta}Ct$ value ($Ct_{\text{gene of interest}} - Ct_{\beta\text{-actin}}$). Relative gene expression was obtained using the $^{\Delta\Delta}Ct$ method ($Ct_{\text{sample}} - Ct_{\text{calibrator}}$) using the *TRPV2$^{flox/flox}$;MerCreMer$^{-/-}$* hearts without tamoxifen as a calibrator.

Histology. Hearts were excised and immediately fixed in buffered 4% paraformaldehyde, embedded in paraffin and sectioned to a thickness of 4 μm. We stained serial sections of samples with Masson's trichrome to evaluate gross morphology and fibrosis. The preparations were examined under a light microscope (SZX7 or BX43, Olympus).

Electron microscopy. For electron microscopy, excised hearts were fixed in 2% paraformaldehyde/2% glutaraldehyde in 0.1 M phosphate buffer, postfixed with 2% OsO4 in 0.1 M phosphate buffer and stained with uranyl acetate and lead citrate. The microtome sections were examined under a JEM-1200 electron microscope (Nihondensi Co., Japan).

Antibodies. The following antibodies were used for immunostaining or immunoblot analysis: anti-TRPV2 (1:200 dilution, AB5398, Millipore); anti-vinculin (1:100 dilution, V9131, Sigma); anti-connexin 43 (1:100 dilution, C6219, Sigma); anti-N-cadherin (1:100 dilution, 3B9, life technologies); anti-Cav3 (1:1,000 dilution, 610420, BD Pharmingen,); anti-LTCC (1:1,000 dilution, ACC033, Alomone); anti-SERCA (1:1,000 dilution, MA3919, Thermo); and anti-RyR (1:1,000 dilution, MA3916, Thermo). The anti-NCX antibody was generated in our laboratory (1:1,000 dilution).

Immunocytochemistry. For immunocytochemistry, 5 μm frozen heart sections embedded in OCT compound (Tissue-Tek) were permeabilized with 0.1% Triton X-100 and incubated with primary antibodies. For immunostaining of rat cardiomyocytes, cells immobilized on collagen-coated glass slides were fixed with 4% paraformaldehyde for 15 min at room temperature, permeabilized with 0.1% Triton X-100 and then stained with primary antibodies.These samples were then treated with Alexa Flour 488-conjugated anti-rabbit IgG (A11008, Life Technologies) or Alexa Flour 488-conjugated anti-mouse IgG (A11001, Life Technologies). Cells or secrions were examined using a confocal microscope (Fluoview FV1000, Olympus) mounted on an Olympus IX81 epifluorescence microscope with a UPlanSApo × 60/1.35 oil immersion objective lens (Olympus).

Immunoblotting. Mice hearts and kidneys were homogenized in a Hiscotron homogenizer (NITI-ON) in lysis buffer containing 20 mM HEPES (pH 7.4), 150 mM NaCl, 1% sodium deoxycholate, 1% SDS, 2 μg ml^{-1} leupeptin, 1 μg ml^{-1} aprotinin, 200 μM phenylmethylsulfonyl fluoride, and 200 μM benzamidine hydrochloride. The lysates were centrifuged at 100,000 *g* for 20 min and the supernatants were used for immunoblot analysis. Immunoreactive bands were visualized using a chemiluminescence detection system (Perkin Elmer) and an LAS3000 Luminescent Image Analyzer (Fuji Film).

Data analysis. Data were analysed by individuals who were blinded to the genotype, drug treatment or operation. Data presented here were reproducible in at least three independent experiments. Results are shown as the mean ± s.e.m. Paired data were evaluated using a Student's *t*-test. Two-way analysis of variance with Bonferroni's *post hoc* test was used for multiple comparisons wherever appropriate. The Kaplan–Meier method with a log-rank test was used for survival analysis. $P < 0.05$ was considered statistically significant.

References

1. Engler, A. J., Sen, S., Sweeney, H. L. & Discher, D. E. Matrix elasticity directs stem cell lineage specification. *Cell* **126,** 677–689 (2006).
2. McCain, M. L. & Parker, K. K. Mechanotransduction: the role of mechanical stress, myocyte shape, and cytoskeletal architecture on cardiac function. *Eur. J. Physiol.* **462,** 89–104 (2011).
3. Hill, J. A. & Olson, E. N. Cardiac plasticity. *New Engl. J. Med.* **358,** 1370–1380 (2008).
4. Estigoy, C. B. *et al.* Intercalated discs: multiple proteins perform multiple functions in non-failing and failing human hearts. *Biophys. Rev.* **1,** 43–49 (2009).
5. Noorman, M. *et al.* Cardiac cell-cell junctions in health and disease: electrical versus mechanical coupling. *J. Mol. Cell. Cardiol.* **47,** 23–31 (2009).